Reliable Open-Phase Fault Detection to Prevent Single-Pole Reclosing Onto Existing Faults

Tomas Enrique Velasco Ramirez and Carlos Alberto Vizcaino Nuñez
Comisión Federal de Electricidad

Sajal Kumar Harmukh, David Schmidt, Emma Clawson,
Omar A. Oliveros, and Jean León Eternod
Schweitzer Engineering Laboratories, Inc.

Presented at the
51st Annual Western Protective Relay Conference
Spokane, Washington
October 22–24, 2024

Reliable Open-Phase Fault Detection to Prevent Single-Pole Reclosing Onto Existing Faults

Tomas Enrique Velasco Ramirez and Carlos Alberto Vizcaino Nuñez, *Comisión Federal de Electricidad*
Sajal Kumar Harmukh, David Schmidt, Emma Clawson, Omar A. Oliveros, and Jean León Eternod,
Schweitzer Engineering Laboratories, Inc.

***Abstract*—Single-pole tripping is a technique employed to clear temporary single-line-to-ground faults on transmission lines while maintaining system stability and power transfer. In the single-pole-open state, electrostatic and electromagnetic coupling from the energized phases (and potentially parallel lines) can sustain the fault on the open phase through the ionized channel created by the primary fault. This phenomenon, known as secondary arcing, can significantly extend the time it takes for the arc to extinguish.**

Existing reclosing schemes typically incorporate a fixed dead time before reclosing. This dead time is an estimate to allow for secondary arcs to extinguish and for dielectric strength to build sufficiently to withstand full nominal phase voltage. However, depending on system and fault characteristics, this dead time may be longer than required. Conversely, the fault might be permanent, or secondary arcing could persist beyond the dead time. In both scenarios, reclosing should be blocked.

To address these challenges, this paper introduces an algorithm that detects faults on the open phase by using only local voltages and currents. Specifically, the algorithm identifies the presence of arcing and bolted faults that persist through the end of the dead time. Additionally, it can detect the extinction of secondary arcing before the dead time expires. The outputs of the algorithm can be used to shorten reclosing dead time when secondary arc extinction is detected or to block reclosing when a fault is still present at the end of the dead time.

The proposed algorithm is applicable to both uncompensated and shunt-reactor-compensated lines and performs well for both transposed and untransposed lines. It requires that the self- and mutual impedances and capacitances of the line be known.

This paper delves into the problem of secondary arcing and existing solutions. It proposes an algorithm to detect faults or secondary arcing on the open phase during single-phase-open conditions. Finally, the paper validates the algorithm's performance against field events and simulations.

I. Introduction

A single-line-to-ground (SLG) fault is the most common fault type in power systems [1]. Because most SLG faults are temporary, single-pole tripping and autoreclosing is commonly used to maintain continuity of service through the healthy phases, improve transient system stability, and allow the temporary fault to clear before reclosing the faulted phase. In most cases, the dead time (i.e., the time between single-pole tripping and autoreclosing) is a fixed interval set to allow enough time for a secondary arc (SA) to extinguish while ensuring system stability.

Secondary arcing refers to sustained arcing through an ionized channel that persists after the primary fault current has been cleared by using single-pole tripping to isolate the faulted phase. An SA is maintained because of capacitive and inductive coupling from the healthy phases.

Several techniques have been proposed to mitigate secondary arcing and reduce the SA extinction (SAE) time. For transposed line applications, these typically include the use of a four-legged shunt reactor with a properly sized neutral reactor [2] [3] [4]. For untransposed lines, References [5] and [6] propose a compensation scheme where a modified four-legged reactor is used in conjunction with a simple four-legged reactor. Transmission lines with either type of shunt-reactor compensation are hereafter referred to as compensated lines, and lines without shunt reactors are referred to as uncompensated. Some papers have proposed a hybrid reclosing scheme where a single-pole trip is followed by a three-pole trip and reclose with a short dead time [1]. The three-pole trip and reclose removes the healthy phase sources feeding the SA and speeds up the extinction process. Another technique uses high-speed grounding switches in each phase on either end of the line, which removes the induced voltage feeding the SA [7]. Use of these techniques can considerably reduce the SAE time so that the dead time can be reduced.

The duration of an SA is dependent on many factors, some of which are not deterministic. The dead time is typically selected to cover the worst-case scenario that leads to the longest arc duration. Due to the nonoptimal nature of a fixed time, there are often situations when the SA extinguishes quickly but the reclosing still has to wait for the dead time to expire. On the other hand, coupling from nearby energized phases or a lack of visibility into the nature of the fault (permanent or temporary) can cause unnecessary recloses onto existing faults. Thus, there is a need for adaptive autoreclosing that can be used to reclose faster for quicker arc extinction or to block reclosing if a permanent fault exists.

Several algorithms have been proposed for adaptive autoreclosing [8]. One approach uses the presence of odd harmonics to detect arcing, and a lack thereof is assumed to be an arc extinction [9] [10] [11]. However, a bolted permanent fault may not produce any harmonics. Moreover, for compensated lines, a subsynchronous ringing frequency after SAE can leak into the harmonic measurements and delay the SAE detection or falsely indicate a permanent fault. Another common technique uses the trajectory of the open-phase voltage angle, Vang [10] [11]. This concept assumes Vang remains outside a sector defined between the healthy phase voltages during secondary arcing and then moves inside the

sector after SAE. However, this approach does not take into account parallel lines, untransposed lines, line loading, or shunt-reactor-compensated lines, all of which can cause the open-phase voltage angle to deviate from the expected behavior. This approach is discussed in more detail later in this paper. A recent method proposes using the long-window derivative of a low-pass filtered (LPF) open-phase voltage magnitude and angle to detect arcing and its extinction [12]. Reference [12] proposes that the derivative is positive during the arcing period and zero or negative during the extinction period or for permanent faults. However, because of the derivative's long window, it may be difficult to distinguish between a short-duration SA and a permanent fault. Further, in compensated transmission lines with properly sized neutral reactors, if there is not enough loading on the healthy phases, the fundamental phasor after SAE contains mostly leakage from the decaying ringing, giving the impression of a downward trend. This condition may be declared as a permanent fault by the algorithm provided in [12]. Reference [13] proposes using different signatures for arc extinction depending on the compensation information. For uncompensated lines, it uses the angle between open-phase voltage and zero-sequence current. For compensated lines, if the compensation level is below a certain level, it uses the open-phase voltage frequency, and if the compensation level is above that level, it uses the open-phase voltage magnitude. As mentioned earlier and in Subsection IV.C.1, the open-phase voltage angle is not a reliable quantity for detecting SAE. Additionally, the compensation level can sometimes change dynamically if there are reactors on either end of the line and one of the reactors is switchable, requiring the reactor service status information from the other end of the line in order to use this approach.

In summary, the existing approaches either assume a transposed line or an uncompensated line, ignore line loading, or use a long window for processing that may miss a faster arc extinction.

In this paper, we present a new algorithm that addresses the problems previously discussed and which reliably detects an existing fault on an open phase, which can in turn be used to block reclosing. Additionally, it can detect SAE before the expiration of the dead time, which could allow for faster reclosing. The algorithm can be used for transposed, untransposed, compensated, and uncompensated lines.

The rest of the paper is organized as follows: Section II provides theoretical background information on behavior of the open-phase voltage during unfaulted and faulted conditions for compensated and uncompensated transmission lines. The detailed derivations are provided in the appendices and the main results are used for discussion. Section II also presents a qualitative discussion on the occurrence of ringing after SAE in compensated lines. Section III presents the proposed algorithm to detect open-phase faults for uncompensated and compensated transmission lines. Section IV discusses the simulation setup and the parameters we varied to thoroughly test the algorithm. It also presents some interesting results that show why relying on the open-phase voltage angle to be in a particular sector is not a reliable way to detect existing faults or SAE. We then discuss the proposed algorithm's performance for simulated permanent and transient faults in uncompensated and compensated lines. Section V presents four field events from CFE: one for an uncompensated line and three for compensated lines (consisting of two temporary faults and one permanent fault). We also evaluate the algorithm's performance for these events. Finally, Appendices A through C provide detailed derivations related to the open-phase voltage, Appendices D and E provide derivations related to voltage ringing for shunt-reactor-compensated lines, and Appendix F discusses the test case parameters and configurations we used in our simulations.

II. Open-Phase Voltage: Theoretical Analysis

Following an SLG fault and subsequent breaker opening of the faulted phase, the line-side PT provides the most direct measurement on the faulted phase. Thus, it is important to analyze the behavior of the open-phase voltage, VOpn, in the presence of bolted and arcing faults as well as after the removal of the fault. This section provides a theoretical analysis of the expected behavior of VOpn. An uncompensated transmission line is considered first, followed by a compensated transmission line with a four-legged reactor bank.

A. Open-Phase Voltage in Unfaulted Uncompensated Transmission Lines

We use a π-model approximation of the transmission line to analyze the open-phase voltage, as shown in Fig. 1. The left side of the circuit is referred to as the sending (or local) end and the related quantities bear the subscript S. The right side is referred to as the receiving (or remote) end and the related quantities bear the subscript R. The circuit includes the phase-to-ground and phase-to-phase admittances. It also includes the voltage induced in each phase because of electromagnetic (EM) coupling from the current in the other two phases. The line is assumed to be untransposed. The transposed line can be treated as a special case of the untransposed line. Phase A is open from both ends, and the SA is assumed to be extinguished. The detailed derivation for VOpn is provided in Appendix A; only some results are referenced here.

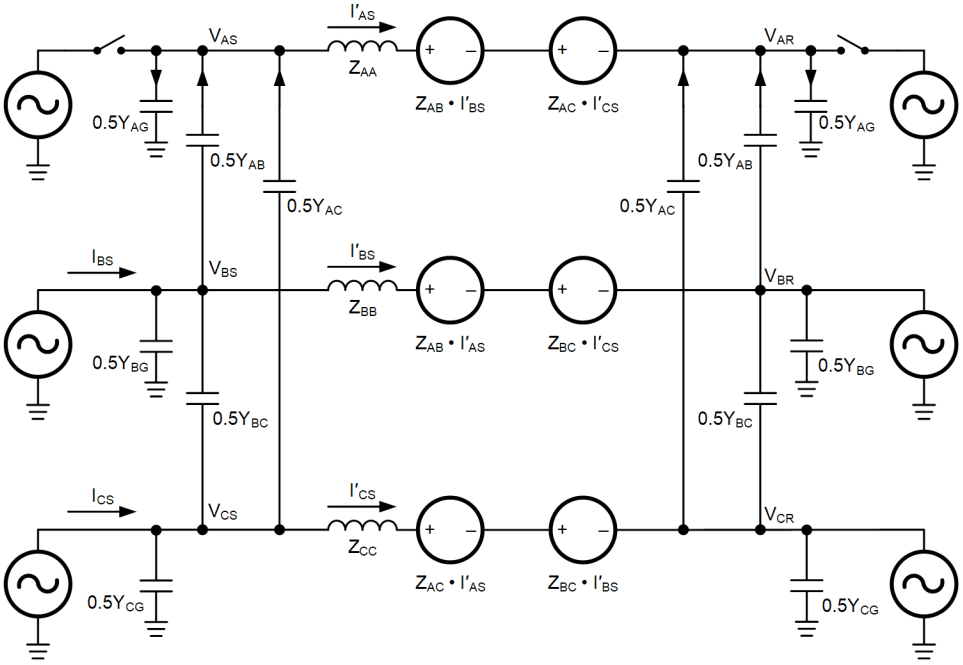

Fig. 1. π-Circuit Representation for an Uncompensated Transmission Line With an Open Phase A

Applying Kirchhoff's current law on Phase A, we get:

$$V_{AS} + V_{AR} = \frac{(V_{BS} + V_{BR})Y_{AB} + (V_{CS} + V_{CR})Y_{AC}}{Y_{AA}} \quad (1)$$

where $V_{[p]S}$ and $V_{[p]R}$ refer to the measured Phase [p] sending and receiving end voltages, respectively; $Y_{[m][n]}$ represents the mutual admittance between Phase [m] and Phase [n]; and $Y_{[pp]}$ represents the sum of admittances connected to Phase [p], which is a diagonal term of the Y_{ABC} matrix corresponding to Phase [p]. Equation (1) represents the electrostatic (ES) component of VOpn.

Applying Kirchhoff's voltage law on Phase A, we get:

$$V_{AS} - V_{AR} = I'_{AS}Z_{AA} + I'_{BS}Z_{AB} + I'_{CS}Z_{AC} \quad (2)$$

where $I'_{[p]S}$ refers to the Phase [p] charging-current-compensated current from the sending end, $Z_{[pp]}$ represents the self-impedance of Phase [p], and $Z_{[m][n]}$ represents the mutual impedance between Phases [m] and [n]. Equation (2) represents the EM component of VOpn. I'_{AS} represents the difference in charging current between the sending and receiving ends. It is relatively small compared to healthy phase load currents and can be ignored. Thus, we can combine (1) and (2) to get:

$$V_{AS} = \frac{V_{B_{avg}}Y_{AB} + V_{C_{avg}}Y_{AC}}{Y_{AA}} + \frac{I'_{BS}Z_{AB} + I'_{CS}Z_{AC}}{2} \quad (3)$$

where $V_{[p]_{avg}}$ refers to the average of the sending- and receiving-end voltage for phase [p]. Let us define the total EM voltage, $V_{EM_{Total}}$, and the ES component of the unfaulted open-phase voltage, $V_{ES_{Unfault}}$, as:

$$V_{EM_{Total}} = I'_{BS}Z_{AB} + I'_{CS}Z_{AC}$$
$$V_{ES_{Unfault}} = \frac{V_{B_{avg}}Y_{AB} + V_{C_{avg}}Y_{AC}}{Y_{AA}} \quad (4)$$

We can see from (3) and (4) that the unfaulted open-phase V_{AS} contains half of $V_{EM_{Total}}$. A single-ended version of (3) can be derived where the receiving-end healthy phase voltages can be expressed in terms of sending-end voltages and currents (see Appendix A). The single-ended approach is used in the magnitude check calculations of the proposed algorithm (see Subsection III.C.4.

B. Open-Phase Voltage in Unfaulted Compensated Transmission Lines

In this section, we analyze the open-phase voltage in a shunt-reactor-compensated line. The shunt reactor bank is assumed to be a four-legged reactor bank available on both ends of the line. The analysis is performed for a transposed line; the compensation scheme for an untransposed line is more complicated, and is covered in [5]. Further, the proposed algorithm does not use the VOpn magnitude for compensated lines; however, we still perform the analysis for transposed compensated lines to explain the reason for this.

Consider the circuit diagram of the unfaulted transposed compensated transmission line as shown in Fig. 2. In the figure, Y_G refers to phase-to-ground capacitive admittance, Y_M refers to mutual capacitive admittance, and L_P and L_N refer to the phase and neutral reactor inductance, respectively. For simplicity, only the left half of the circuit is shown. The reactor values are equally distributed between both line ends and show up as twice the values used for sizing the reactor. A detailed derivation for VOpn is provided in Appendix B; only some results are shown here for discussion.

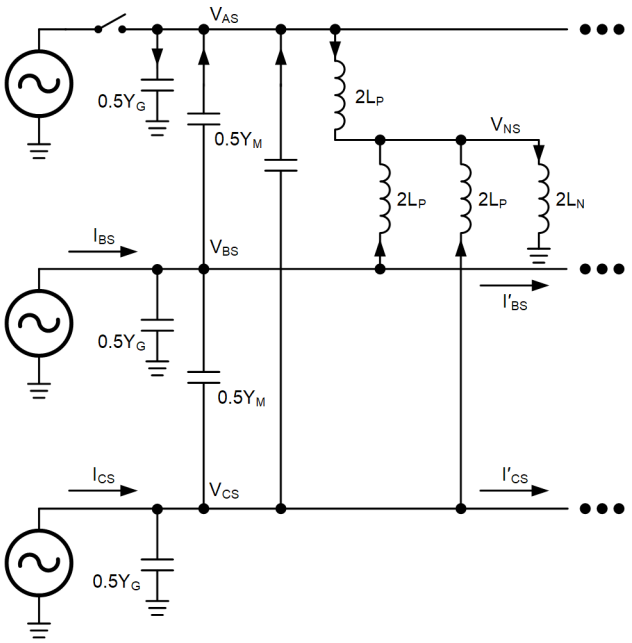

Fig. 2. π-Circuit Representation for a Compensated Transmission Line With an Open Phase A

Applying Kirchhoff's current law on Phase A and simplifying (see Appendix B), we get:

$$V_{AS} + V_{AR} = \frac{\left(V_{BS} + V_{BR}\right)Y'_M + \left(V_{CS} + V_{CR}\right)Y'_M}{Y'_S} \tag{5}$$

where the primed (′) parameters are defined in (6).

$$\begin{aligned} Y'_S &= Y_S + \frac{Z_P + 2Z_N}{Z_P\left(Z_P + 3Z_N\right)} \\ Y'_M &= Y_M + \frac{Z_N}{Z_P\left(Z_P + 3Z_N\right)} \end{aligned} \tag{6}$$

Y_S refers to the self-admittance, which is equal to $Y_G + 2Y_M$, and Z_P and Z_N refer to the phase and neutral reactor impedances, respectively. In (6), for both equations, note that we are adding capacitive and inductive admittances, which tend to cancel each other and reduce the original admittance. This, in turn, reduces the ES component of the recovery voltage and the SAE time. The size of the neutral reactor that fully compensates the mutual capacitance can be determined by forcing Y'_M in (6) to 0 (see Appendix B). If a properly sized neutral reactor is selected, the ES component (i.e., the right side of (5)) becomes 0.

Applying Kirchhoff's voltage law on Phase A, we get:

$$V_{AS} - V_{AR} = \left(I'_{BS} + I'_{CS}\right)Z_M \tag{7}$$

where $I'_{[p]S}$ refers to the charging-current and reactor-current compensated Phase [p] current (see Appendix B for more details) and Z_M represents the mutual impedance between the phases.

Equations (5) and (7) can be combined to provide the open-phase voltage, as shown in (8).

$$V_{AS} = \frac{\left(V_{B_{avg}} + V_{C_{avg}}\right)Y'_M}{Y'_S} + \frac{\left(I'_{BS} + I'_{CS}\right)Z_M}{2} \tag{8}$$

If a neutral reactor is sized to completely compensate the mutual capacitance, the ES component becomes negligible, and (8) can be written as:

$$V_{AS} = \frac{\left(I'_{BS} + I'_{CS}\right)Z_M}{2} \tag{9}$$

Equation (9) shows that for compensated lines where the neutral reactor is properly sized to compensate the mutual capacitance, the VOpn magnitude is highly dependent on the line loading and can be very small, e.g., less than 1 percent of nominal voltage for an unloaded line, or significant, e.g., as high as 10 percent of nominal voltage for highly loaded lines, as observed from simulations. Additionally, if two reactor banks are employed, one at each end of the line, and one of the reactors is switchable, removing one of the reactors results in an unbalance where the remaining neutral reactor is no longer adequately sized to offset the mutual capacitance. This can cause the VOpn magnitude to increase to 20 percent of the nominal voltage, as observed in simulations. This variability, coupled with the reliance of the VOpn magnitude on the correct sizing of the neutral reactor and the status of a switchable reactor, is why a magnitude check is not suitable for detecting open-phase faults in compensated lines.

C. Open-Phase Voltage in Uncompensated Lines During Faults

Let us assume that a fault exists on the open Phase A at location m per-unit line length from the sending end of an untransposed and uncompensated transmission line. The circuit diagram from the sending end to the fault point is shown in Fig. 3. The open-phase related admittances and impedances are scaled by m.

The open-phase voltage is derived in Appendix C, resulting in (10).

$$V_{AS} = V_{ES_{Fault}} + V_{EM_{Fault}} + V_{Rf} \tag{10}$$

Here, $V_{ES_{Fault}}$ is the ES component, $V_{EM_{Fault}}$ is the EM component, and V_{Rf} is the resistive-fault component of the faulted open-phase voltage. These three variables are defined in (11).

$$\begin{aligned} V_{ES_{Fault}} &= \frac{m\left(Y_{AB}V_{BS} + Y_{AC}V_{CS}\right)\left(mZ_{AA} + R_f\right)}{1 + mY_{AA}\left(mZ_{AA} + R_f\right)} \\ V_{EM_{Fault}} &= \frac{m\left(Z_{AB}I'_{BS} + Z_{AC}I'_{CS}\right)}{1 + mY_{AA}\left(mZ_{AA} + R_f\right)} \\ V_{Rf} &= \frac{R_f I_{AR}}{1 + mY_{AA}\left(mZ_{AA} + R_f\right)} \end{aligned} \tag{11}$$

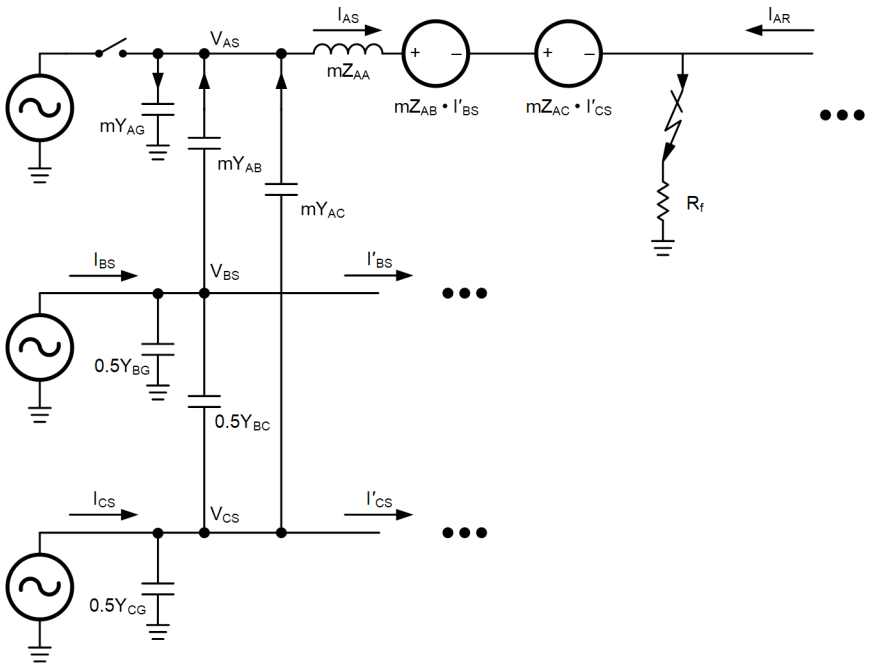

Fig. 3. π-Circuit Representation of an Uncompensated Transmission Line During a Fault

For a bolted fault, R_f is 0 and the definitions in (11) become:

$$V_{ES_{Fault}} = \frac{m^2 Z_{AA}\left(Y_{AB}V_{BS} + Y_{AC}V_{CS}\right)}{1 + m^2 Y_{AA}Z_{AA}}$$
$$V_{EM_{Fault}} = \frac{m\left(Z_{AB}I'_{BS} + Z_{AC}I'_{CS}\right)}{1 + m^2 Y_{AA}Z_{AA}} \quad (12)$$
$$V_{Rf} = 0$$

Let us compare the bolted-fault and unfaulted open-phase voltage magnitude. We start by comparing the ES components of the unfaulted and bolted-fault open-phase voltages (i.e., $V_{ES_{Unfault}}$ (4) and $V_{ES_{Fault}}$ (12)). For simplicity, we can assume the sending and receiving voltages are the same (i.e., $V_{BS} = V_{BR} = V_B$ and $V_{CS} = V_{CR} = V_C$). Then we can rewrite $V_{ES_{Unfault}}$ as:

$$V_{ES_{Unfault}} = \frac{Y_{AB}V_B + Y_{AC}V_C}{Y_{AA}} \quad (13)$$

The relative magnitude can be analyzed by taking the ratio of the two quantities as:

$$ES_{Fault_{pu}} = \frac{V_{ES_{Fault}}}{V_{ES_{Unfault}}} = \frac{m^2 Z_{AA}Y_{AA}}{1 + m^2 Z_{AA}Y_{AA}} \quad (14)$$

The magnitude of the $Z_{AA}Y_{AA}$ term in (14) is much smaller than 1, making $ES_{Fault_{pu}}$ very small. Fig. 4 plots the $ES_{Fault_{pu}}$ for a 400 kV untransposed transmission line for a 30 km line and a 100 km line for values of m ranging from 0 to 1. It can be seen that the ratio is very small, which shows that the ES component is negligible during a bolted fault and that the open-phase voltage during the bolted fault is essentially equal to the EM component.

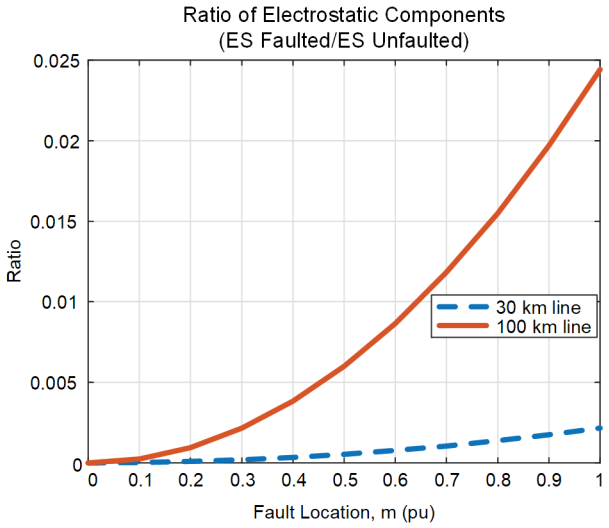

Fig. 4. Electrostatic Components Ratio of Faulted and Unfaulted Open-Phase Voltage for Various Fault Locations (m) on a 30 km Line and a 100 km Line

Because the ES component of the bolted-fault voltage is negligible, we compare the EM component of the bolted-fault voltage, $V_{EM_{Fault}}$ (12), to the total unfaulted open-phase voltage (3). We begin by comparing $V_{EM_{Fault}}$ to the EM component of the unfaulted voltage. Recall that $Z_{AA}Y_{AA}$ is very small, so we can replace the denominator in (12) with 1. This simplifies the expression for $V_{EM_{Fault}}$ as:

$$V_{EM_{Fault}} \approx m\left(Z_{AB}I'_{BS} + Z_{AC}I'_{CS}\right) = m \bullet V_{EM_{Total}} \quad (15)$$

where $V_{EM_{Total}}$ is defined in (4). When m = 1, $V_{EM_{Fault}}$ becomes equal to the total EM voltage $V_{EM_{Total}}$, whereas the EM component of the unfaulted open-phase voltage in (3) is always half of $V_{EM_{Total}}$. In other words, for midline faults, the EM

component of the bolted-fault open-phase voltage is equal to the EM component of the unfaulted open-phase voltage; for close-in faults it is smaller, and for end-of-line faults it is larger.

The comparison between $V_{EM_{Fault}}$ and $V_{ES_{Unfault}}$ (4) is less straightforward. To analyze that relationship, and the overall relationship between $V_{EM_{Fault}}$ and the total unfaulted voltage, we consider the example of a 100 km, 400 kV untransposed line. Fig. 5 compares the magnitudes of $V_{EM_{Fault}}$, $V_{ES_{Unfault}}$, and the measured total unfaulted voltage (3) at various levels of line loading. For $V_{EM_{Fault}}$, the fault location is m = 0.9 pu.

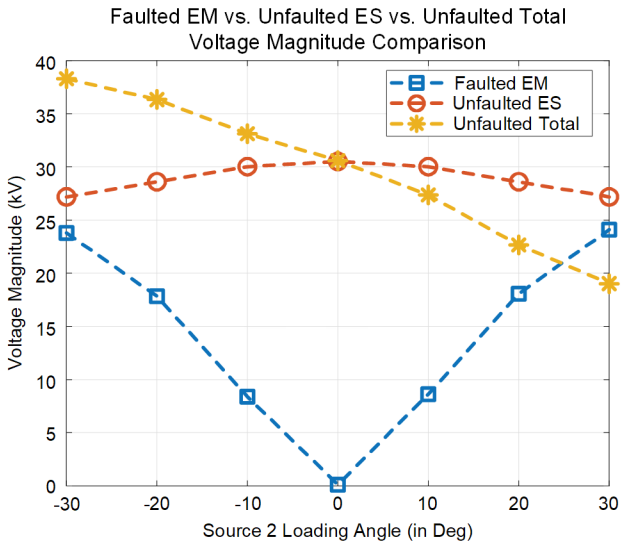

Fig. 5. Magnitude Comparison Between Bolted-Fault EM, Unfaulted ES, and Total Unfaulted Open-Phase Voltage for a 400 kV Untransposed Transmission Line

We can see from Fig. 5 that for higher loading, the magnitude of the faulted EM ($V_{EM_{Fault}}$) reaches as high as 24 kV, which is about 90 percent of the magnitude of the unfaulted ES ($V_{ES_{Unfault}}$) for the same loading (27 kV). If the fault had been at m = 1.0 pu, this percentage would have been even higher. Fig. 5 also shows that the total unfaulted voltage deviates from $V_{ES_{Unfault}}$ in proportion to the amount and direction of line loading. It has a higher magnitude for forward loading (negative remote voltage angles) and a lower magnitude for reverse loading (positive remote voltage angles). This variation is because the total unfaulted voltage (3) contains an EM component (4) that can add to or subtract from $V_{ES_{Unfault}}$, depending on the line loading direction. Of particular interest is the 30-degree point (high reverse loading) where the total unfaulted voltage magnitude is less than $V_{EM_{Fault}}$.

In summary, during faults, the ES component is negligible, whereas the EM component can be as much as twice as high as in the unfaulted case. Additionally, the EM component for faulted VOpn can be as high as the ES component for the unfaulted case. Finally, certain loading directions can cause the EM component to be subtracted from the ES component in the unfaulted state, which can result in a lower overall voltage than the bolted-fault case.

D. Analysis of Ringing in Shunt-Reactor-Compensated Transmission Lines

In this section, we provide a qualitative explanation for why SAE in a shunt-reactor-compensated transmission line is always accompanied by a subsynchronous ringing in the open-phase voltage. Refer to the simplified equivalent circuit diagram of a shunt-reactor-compensated transposed transmission line as shown in Fig. 6. In this circuit, C_G refers to phase-to-ground capacitance, C_M refers to mutual phase capacitance, L_P refers to phase reactor inductance, L_N refers to neutral reactor inductance, and R_{ARC} refers to fault arc resistance. See Appendix D for a derivation of this equivalent circuit. R_{ARC} is shown as a variable resistance that increases with time as the arc lengthens. The voltage across the parallel combination is the open-phase voltage, VOpn. When the arc extinguishes at a current zero-crossing, VOpn is also zero at that instant. This condition implies that there is no energy in the capacitor; however, the point in time at which there is zero voltage across the inductor is also the instant when maximum current flows through it and peak energy is stored in it ($E = 1 / 2Li^2$). With the resistor removed, after SAE, the LC combination resonates with the stored energy in the inductor L, leading to ringing in the voltage. The frequency of the oscillation can be approximately determined from (16), where $Comp_{pu}$ refers to the per-unit positive-sequence shunt-reactor compensation (see Appendix D).

$$F_{RING} = F_{NOM}\sqrt{Comp_{pu}} \tag{16}$$

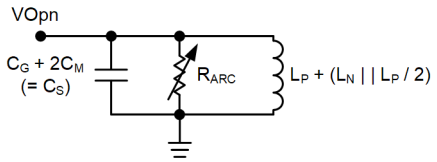

Fig. 6. Equivalent Circuit to Study Ringing

Subsections II.A, II.B, and II.C provide a mathematical analysis of the open-phase voltage behavior for uncompensated and compensated lines during unfaulted and faulted states. They identified the EM and ES contributions to the open-phase voltage. For a compensated line, it was shown that the open-phase voltage magnitude is highly variable and dependent on neutral reactor sizing, the switching status of a switchable reactor, and line loading. Consequently, the open-phase voltage magnitude of a compensated line is not a reliable quantity to determine the fault status on the open phase. The analysis for the bolted fault showed that it is possible for the bolted-fault open-phase voltage magnitude to become higher than the unfaulted open-phase voltage magnitude under certain circumstances. This can pose problems when using the magnitude of the open-phase voltage to determine if a fault exists on the open phase. We discuss a solution to this problem in Subsection III.C.4 and use that as one of the SAE detection criteria for uncompensated lines. The qualitative analysis on ringing showed that SAE in compensated transmission lines is always accompanied by ringing. This fact is used for SAE detection in compensated lines in Subsection III.D.2.

III. Proposed Method for Open-Phase Fault Detection

This section presents the proposed algorithm for open-phase fault detection in uncompensated and shunt-reactor-compensated transmission lines. The underlying principle of the algorithm is described first, followed by its detailed description.

A. Underlying Principle of SAE Detection

Fig. 7 shows the pre-fault, primary fault, secondary arcing, and reclosed states from an actual field event on a 162 km, 230 kV parallel line. The signals shown are the fundamental frequency voltage magnitude of the open phase (blue trace) and the root-mean-square (rms) sum of the second through fifth harmonics of the open phase (red trace). In this event, the faulted phase experienced an SLG fault, followed by faulted-phase isolation, secondary arcing, arc extinction, and successful reclosure. Note that the left y-axis corresponds to the fundamental frequency phasor magnitude plot and the right y-axis pertains to the rms harmonic sum plot.

Following the breaker opening, the voltage magnitude initially decreases because of the removal of the primary source and then increases as the SA lengthens. The arcing state is marked by significant distortion due to harmonics, interharmonics, and higher frequencies. When the SA extinguishes, the voltage becomes clean (the rms harmonic sum decreases to nearly zero) and its magnitude stabilizes.

These observations provide the foundation for the core principles of our algorithm. A peak tracker monitors the movement of the fundamental frequency voltage magnitude, while a harmonic distortion calculator estimates the harmonic content as an rms sum of the second through fifth harmonics. A magnitude comparator checks a compensated voltage against a calculated threshold for uncompensated lines (see Subsection II.C), while a ringing detector identifies ringing for compensated lines. When the algorithm detects no new peaks, harmonics fall below a preset threshold, and either the voltage magnitude exceeds a threshold check (for uncompensated lines) or the algorithm detects ringing (for compensated lines), arc extinction is declared. A failure of any of these checks just before the dead time expires can be used to block an impending reclose attempt. There are some additional considerations for harmonic detection when shunt reactors are installed, which are described later in Subsection III.D.

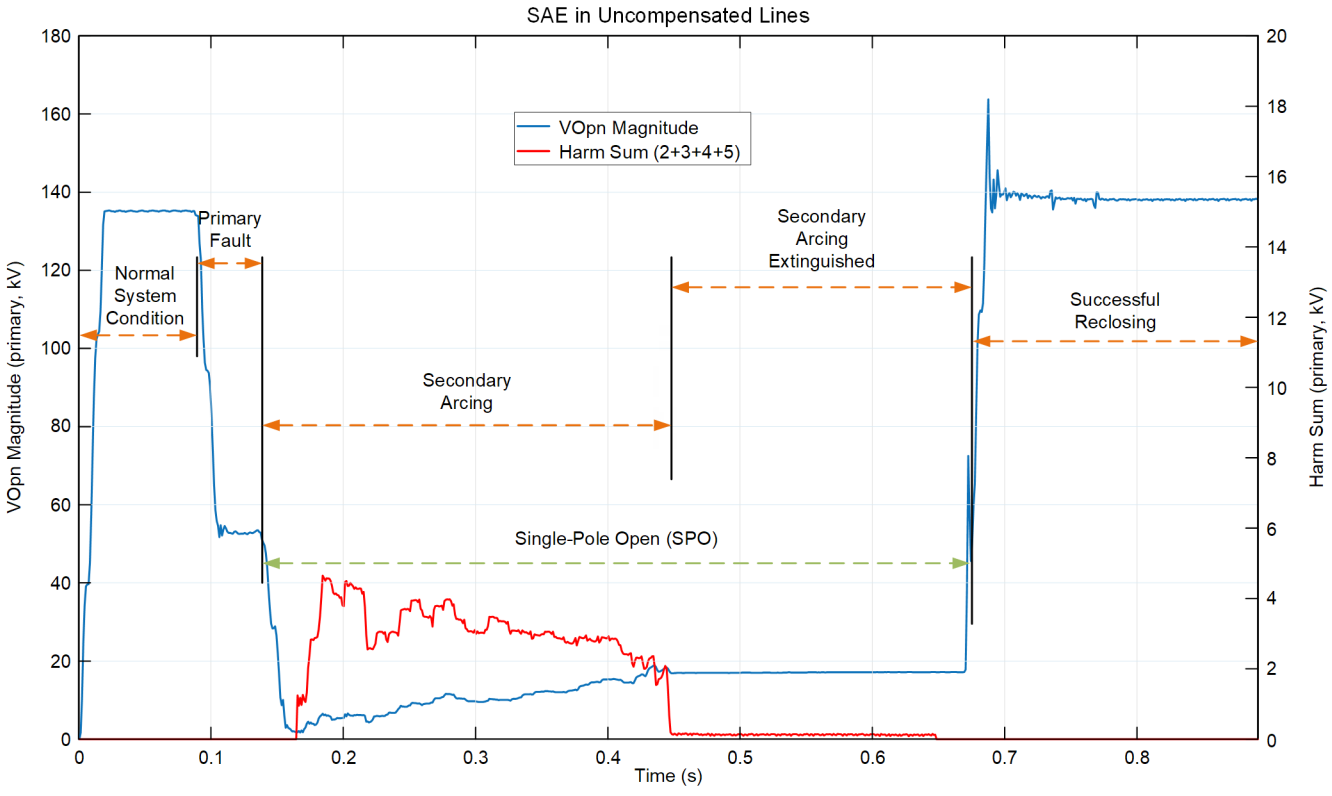

Fig. 7. SAE in the Absence of Shunt Reactors

B. Filtering for Open-Phase Voltage

The open-phase voltage is filtered to extract the fundamental frequency magnitude and its second through fifth harmonic components. It is important to note that the phasor filter used is a correlator where the phase relationship between the coefficients and the signal is preserved. This results in static real and imaginary phasor components as opposed to using a regular one-cycle filter like a cosine or fourier filter where filtered quantities rotate at their original frequency. The fundamental frequency magnitude undergoes further processing through a first-order, low-pass Butterworth filter, which effectively attenuates higher frequency components so the algorithm can work with the underlying trends in the signals. The output of the low-pass filter is the open-phase voltage magnitude, VOpn_Mag_LP, which is used by the rest of the algorithm. This filtering process is common to scenarios with and without shunt-reactor compensation. Additional filtering is required to handle ringing when shunt reactors are present; see Subsection III.D for details.

C. Adaptive Reclosing Algorithm in the Absence of Shunt Reactors

In the absence of shunt reactors, the algorithm consists of six blocks: arming logic, minima tracker, peak tracker, harmonic distortion calculator, magnitude comparator, and secondary arc extinction detector (SAED). These blocks are shown in Fig. 8 and are described in more detail below.

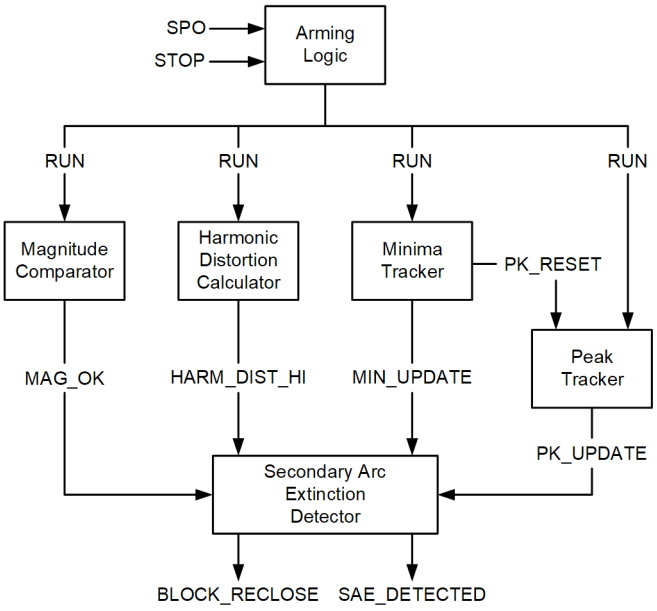

Fig. 8. Block Diagram of the SAED Algorithm (in the Absence of Shunt Reactors)

1) Arming Logic

Arming logic arms the algorithm by using the RUN bit when a single-pole open (SPO) condition occurs, as shown in Fig. 9. The SPO signal is delayed to allow the phasors to stabilize. A STOP bit, which could be a combination of a CLOSE command and a recloser lockout signal, disarms the logic.

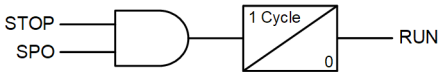

Fig. 9. Arming Logic for SAED Algorithm

2) Minima and Peak Tracker

The minima and peak trackers track the minimum and peak values of VOpn_Mag_LP and assert MIN_UPDATE and PK_UPDATE when a new minimum or peak is found, respectively. MIN_UPDATE resets the peak tracker so it does not capture a high value when VOpn_Mag_LP decreases from the primary fault value.

3) Harmonic Distortion Calculator

The harmonic distortion calculator combines the second, third, fourth, and fifth harmonic components of the open-phase voltage into an rms sum (17). When the harmonic distortion is greater than a default fraction (0.05; i.e., 5 percent) of the fundamental frequency component, the output HARM_DIST_HI asserts.

$$\text{Harm\_Dist} = \sqrt{\text{VOpn}_{H2}^2 + \text{VOpn}_{H3}^2 + \text{VOpn}_{H4}^2 + \text{VOpn}_{H5}^2} \quad (17)$$

4) Magnitude Comparator

The magnitude check differentiates an unfaulted state from a faulted state with no harmonics. As discussed in Subsection II.C, a direct comparison between a threshold and VOpn_Mag_LP may not conclusively distinguish between the faulted and unfaulted state because the faulted voltage magnitude may exceed the unfaulted voltage magnitude. To solve this, we subtract half of the total induced EM voltage, $V_{EM_{Total}}$ (see (4)) from the measured VOpn. If the arc is extinguished, this subtraction removes the EM component, leaving only the ES component of VOpn. If the fault is bolted, the subtraction limits VOpn to half of $V_{EM_{Total}}$. With the unfaulted VOpn reduced to just the ES component and the faulted VOpn restricted to half of $V_{EM_{Total}}$ (which in turn can be as high as the ES component) after subtraction, a threshold of more than 50 percent of the estimated ES component provides a good way to compare the compensated voltages. We chose a default value of 85 percent of the estimated ES component as the threshold. The total EM voltage can be estimated either accurately or approximately, as shown in (18), depending on whether the accurate mutual impedance parameters are available or not, respectively.

$$\text{VOpn}_{EM_{Total}} = \begin{cases} I'_{BS} \bullet Z_{AB} + I'_{CS} \bullet Z_{CA} \,(\text{accurate}) \\ (I'_{BS} + I'_{CS}) \bullet Z_M \,(\text{approximate}) \end{cases} \quad (18)$$

The open-phase voltage is compensated as shown in (19).

$$\text{VOpn}_{Comp} = \text{VOpn}_{Meas} - \frac{\text{VOpn}_{EM_{Total}}}{2} \quad (19)$$

The compensated magnitude, VOpn_{Comp}, is compared to a default threshold of 85 percent of the estimated ES voltage calculated in (20). Depending on the availability of mutual capacitances, an accurate or approximate expression can be used. The average of the local and estimated remote healthy phase voltages (see Appendix A, (31), and (32)) is used.

$$VOpn_{ES_{Est}} = \begin{cases} \dfrac{V_{B_{avg}} \bullet C_{AB} + V_{C_{avg}} \bullet C_{CA}}{C_{AA}} \text{(accurate)} \\ \dfrac{C_M \bullet \left(V_{B_{avg}} + V_{C_{avg}} \right)}{C_S} \text{(approximate)} \end{cases} \quad (20)$$

Equation (21) is used to calculate the magnitude check threshold.

$$Mag\_Check\_Thresh = 0.85 \bullet VOpn_{ES_{Est}} \quad (21)$$

When the compensated open-phase voltage is greater than the magnitude threshold, the MAG_OK bit asserts. It is important to note that such a magnitude comparator can be easily extended to parallel line cases, provided all the signals (currents and voltages) from the parallel line and all the line parameters (including any mutual impedances and admittances between the parallel lines) are available.

5) Secondary Arc Extinction Detector

The SAE_DETECTED logic declares that the SA has extinguished when the following conditions are satisfied for 3 cycles:

- No new peak has been found
- No new minimum has been found
- Harmonic distortion is less than 5 percent of fundamental frequency voltage
- The compensated voltage ($VOpn_{Comp}$) is greater than Mag_Check_Thresh

The 3-cycle pickup delay is required to ensure the above conditions do not result in a reclose being issued based on transients. Furthermore, the SA extinguishing only means that the dielectric strength of the ionized channel has enough strength to withstand the recovery voltage, which can be anywhere from 9 percent to 25 percent of the nominal voltage (as observed from the simulations) for an uncompensated line. The dielectric strength of the ionized channel is not immediately able to sustain the full nominal phase voltage plus any closing transient voltages. Therefore, the 3-cycle time delay is provided to allow sufficient dielectric buildup of the ionized channel [14] [15]. Reference [14] experimentally observed that for a 760 kV line, the recovery voltage rose to nominal voltage in just under 3 cycles after the SA extinguished. This time can be increased by the user if desired. Reference [15] provides an empirically derived formula for estimating the recovery voltage as a function of time after arc extinction assuming worst-case ambient conditions (e.g., still-air conditions, etc.). The logic for SAE_DETECTED is shown in Fig. 10.

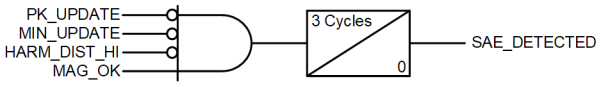

Fig. 10. SAED Algorithm in the Absence of Shunt Reactors

Two milliseconds before the dead time expires, the BLOCK_RECLOSE logic determines if the harmonic distortion is high or if the magnitude check has failed. If either of these two conditions have existed for 3 cycles, the logic indicates that either the SA has not extinguished or the fault is permanent, and if the breaker recloses it will reclose onto the fault. When the arming logic issues the STOP signal, BLOCK_RECLOSE is disabled. Fig. 11 provides the logic for the BLOCK_RECLOSE output.

The SAE_DETECTED and BLOCK_RECLOSE outputs are intended for use in adaptive reclosing logic. SAE_DETECTED can be used as a supervisory signal to allow closing at the end of the reclosing dead time. Alternatively, because SAE_DETECTED can assert at any time during the open interval, it can be used to initiate a close command before the expiration of the dead time. When SAE_DETECTED is used to adaptively reduce the dead time, care should be taken not to exceed the circuit breaker duty cycle rating [16]. BLOCK_RECLOSE assertion can indicate either a prolonged SA or a permanent fault. Consequently, it can be used to block the single-pole reclose and convert to a three-pole trip and reclose.

SAE_DETECTED and BLOCK_RECLOSE are not mutually exclusive. It is not possible for both outputs to be *asserted* concurrently, but it is possible for both to be *deasserted* concurrently, specifically when the SAE_DETECTED conditions are met but the output is still timing. When neither SAE_DETECTED nor BLOCK_RECLOSE are asserted at the end of the dead time, the reclose cycle could be extended by a short time (no longer than the pickup delay on the SAE_DETECTED output) to improve the chances of a successful reclose. Alternatively, the single-pole reclose could be converted to a three-pole trip and reclose.

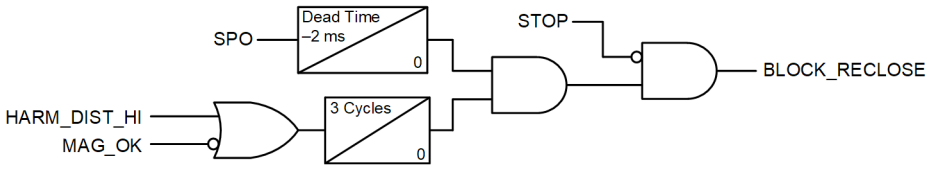

Fig. 11. Block Reclose Logic in SAED (in the Absence of Shunt Reactors)

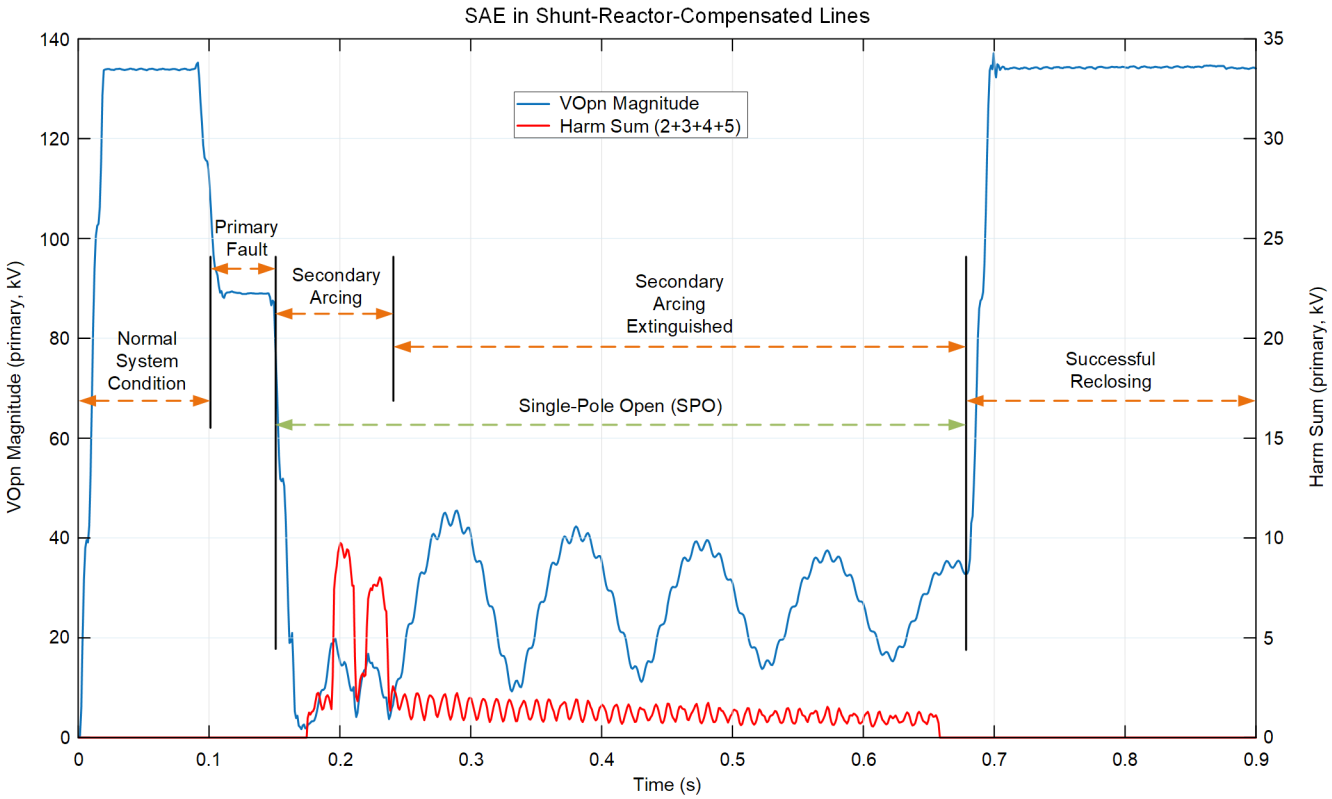

Fig. 12. SAE in the Presence of Shunt Reactors

D. *Adaptive Reclosing Algorithm When Shunt Reactors Are Installed*

1) *Additional Considerations When Shunt Reactors Are Installed*

Fig. 12 shows the pre-fault, primary fault, secondary arcing, and reclosed states from an actual field event on a compensated 230 kV, 145 km parallel transmission line. The signals shown are the fundamental frequency voltage magnitude of the open phase (blue trace) and the rms of the harmonics of the open phase (red trace). In this event, the faulted phase experienced an SLG fault, followed by faulted phase isolation, secondary arcing, arc extinction, and successful phase reclosure. The left y-axis corresponds to the blue fundamental frequency phasor magnitude plot and the right y-axis pertains to the red rms harmonic sum plot.

The following are key differences in open-phase voltage behavior on lines with shunt reactors installed and the modifications to our proposed algorithm to account for them.

- The recovery voltage magnitude is heavily dependent on how well the neutral reactor is sized. When the shunt-reactor compensation is split between the two ends of the line, the recovery voltage magnitude is also dependent on whether one of the shunt reactor banks is switched out at the time of secondary arcing. The variation in the recovery voltage is quite wide, ranging from less than 1 percent to 20 percent of nominal voltage depending on many factors including switch status of each set of shunt reactors, tower configuration, line length, and line loading. Because the voltage magnitude can be very low, but vary widely after SAE, using a magnitude check in the algorithm is no longer reliable. The algorithm can also be applied to shunt-reactor-compensated parallel lines.
- The open-phase voltage magnitude after SAE consists of two components: a steady-state fundamental frequency component due to ES and EM coupling from the other two phases and a transient oscillatory component due to resonance between the shunt reactors and the line capacitance, often referred to as ringing. We can calculate the ringing frequency by using (16). Because of the phasor creation process, the fundamental component shows up as a stationary phasor whereas the ringing component shows up as a rotating phasor with a beat frequency of $F_{NOM} - F_{RING}$. Therefore, averaging the open-phase voltage phasor over one beat frequency cycle removes the ringing component. Instead of a magnitude comparator, we use a ringing detector (see Subsection III.D.3) for compensated lines to determine if the SA has extinguished.
- The ringing in the open-phase voltage also leaks through the harmonic filtering and contributes to the Harm_Dist calculations. This could falsely assert the harmonic distortion detector designed for uncompensated lines. The harmonic distortion calculator needs to either remove the effect of leakage due to ringing or adapt the threshold to accommodate the increase in the harmonic distortion. We adopt the latter approach, which is described in more detail in Subsection III.D.6.

Fig. 13 shows the modified algorithm for when shunt reactors are present. The new blocks and the modified blocks are explained in subsequent sections.

2) Ringing Frequency and Magnitude Estimator

Calculating the amplitudes of the transient ringing component and the fundamental component of the open-phase voltage is crucial to adaptively update the harmonic threshold. When reactor banks are installed at both ends of the line and one of these reactors is switchable, the ringing frequency will change depending on the reactor switch status. Instead of relying on a fixed setting, the algorithm measures the frequency and magnitude of the transient ringing component.

To estimate the ringing component, the algorithm uses a differentiator-smoother filter to remove DC and 60 Hz fundamental voltage and its harmonics. After applying this filter, only the transient ringing portion of the open-phase voltage remains. The ringing frequency is estimated by using zero-crossing detection on the cleaned signal. The ringing signal magnitude is then estimated by obtaining a quarter-cycle delayed sample and creating a phasor. Gain compensation from the filters is used to obtain the true magnitude of the ringing component in the open-phase voltage, V_{RING}.

3) Ringing Detector

The ringing detector block aids in differentiating between a bolted permanent fault and an SA extinguished state. If the fault is bolted, no ringing will occur. If the SA is extinguished, ringing will be present. In the absence of a magnitude check, the harmonics serve as a good indicator of the presence of an arcing fault. However, in scenarios with very-low-resistance faults, such as a bolted fault, harmonics might not be present. In such situations, ringing can be detected, latched on to, and used as an indicator that the SA was extinguished.

To detect ringing, we require the frequency to be within an expected range, determined by typical shunt-reactor compensation levels, and within 1 Hz for the last 5 measurements. The output of this logic is denoted as CONT_RING (short for continued ringing detection). The rising-edge of CONT_RING is latched and denoted as RING_DET.

4) Pausing Minima Tracker for Continued Ringing

It can be seen from (9) that if a shunt-reactor-compensated line is compensated with a properly sized neutral reactor, VOpn contains only the EM component. Under lightly loaded or no-load conditions, the fundamental frequency voltage component may be very low. When ringing occurs in this situation, VOpn contains mostly leakage from the ringing. Because ringing frequency is a subharmonic of the fundamental frequency, ringing will not be removed by phasor filtering and will leak into the phasor. Furthermore, because ringing decays with time, it will cause the phasor magnitude to also decrease, which in turn will cause the minima tracker to assert. Therefore, the CONT_RING bit pauses the minima tracker as long as ringing continues.

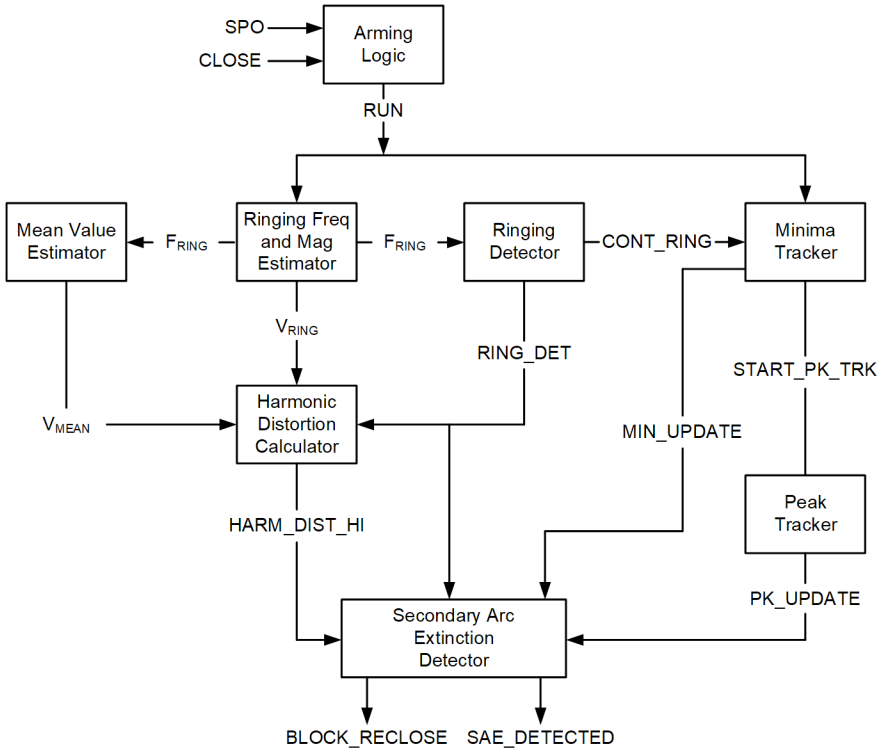

Fig. 13. Block Diagram of the SAED Algorithm (in the Presence of Shunt Reactors)

5) Mean Value Estimator

The open-phase voltage phasor after SAE, by virtue of using a correlator for the phasor filter, consists of a static component (representing the fundamental frequency component) and an oscillatory component (oscillating at beat frequency because of the ringing component). The mean value, V_{MEAN}, of the open-phase voltage phasor therefore represents the fundamental frequency voltage and is used as the threshold for the harmonic distortion comparison after ringing is detected.

V_{MEAN} is extracted by passing the VOpn phasor through an averager filter designed to remove the beat frequency oscillations and then taking its magnitude. This mean value, in conjunction with the ringing voltage magnitude, V_{RING}, is used to adaptively adjust the harmonic threshold, described in the next section.

6) Harmonic Distortion Calculator When Shunt Reactors Are Present

When ringing leaks into the harmonic calculation, the harmonics may become larger than the default threshold, i.e., 5 percent of V_{MEAN}, which would delay the algorithm from declaring SAED until the ringing decays. To prevent such a delay, the harmonic threshold is adaptively raised by a leakage factor, LkgFact, which is derived in Appendix E.

$$V_{HARM_{Meas}} > 0.05 \bullet V_{MEAN} + LkgFact \bullet V_{RING} \qquad (22)$$

The value of V_{MEAN} takes one cycle of the beat frequency to stabilize. Shunt-reactor compensation levels typically do not exceed 75 percent (corresponding to 52 Hz ringing and 8 Hz beat frequency). At 8 Hz, one cycle of beat frequency corresponds to only 7.5 cycles of 60 Hz. Taking into account the 3-cycle qualifying time, SAE can be detected in 10.5 cycles. For lower compensation levels, this time is shorter. After the ringing frequency is measured, the harmonic detection block waits one beat frequency cycle before using V_{MEAN} in its calculation. Before V_{MEAN} stabilizes, the harmonic sum is compared against 5 percent of the minimum tracked value, V_{MIN} (refer to Subsection III.C.2). This secures the algorithm by making the harmonic threshold sensitive until V_{MEAN} stabilizes.

7) Secondary Arc Extinction Detector Logic When Shunt Reactors Are Present

The SA is declared extinguished when ringing is detected, no harmonics are detected, and the voltage magnitude is steady. The BLOCK_RECLOSE bit asserts if harmonics are persistent or if no ringing is detected, as shown in Fig. 14.

IV. Simulation Setup, Results, and Discussions

We performed Electromagnetic Transients Program (EMTP) simulations to validate the algorithm for various transmission line configurations with and without shunt-reactor compensation. This section describes the simulation setup, the types of simulations performed, and results of the simulations. In all cases, the algorithm correctly blocks reclosing for faults present at the end of the dead time or detects SAE within the dead time.

A. Simulation Setup

We used MATLAB Simulink to model a two-terminal transmission line. We measured and processed currents and voltages from one end of the transmission line by using typical protective relay data acquisition methods and fed the results into the algorithm previously described. A control script interface is used to vary the model parameters systematically in order to verify the algorithm response over various combinations of a range of system configurations. The following subsections describe aspects of the model that we varied for the simulations.

1) Transmission Line Parameters

We modeled the transmission line with different tower configurations and voltage levels ranging from 132 kV to 765 kV. We simulated each line type as both transposed and untransposed and varied line length from 30 km to 500 km. Details of the transmission tower configurations and line parameters are included in Appendix F.

2) Shunt-Reactor Compensation

For transposed lines, we modeled four-legged shunt reactors at each end of the transmission line, with the neutral reactor sized according to the equations in Appendix B. For untransposed lines, we modeled a simple four-legged shunt reactor at the local end of the transmission line and a switched four-legged shunt reactor at the remote end [5] [6]. We varied the positive-sequence compensation between 50 percent and 90 percent and connected the shunt reactors through breakers so that each configuration can be simulated with none, one, or both reactors connected.

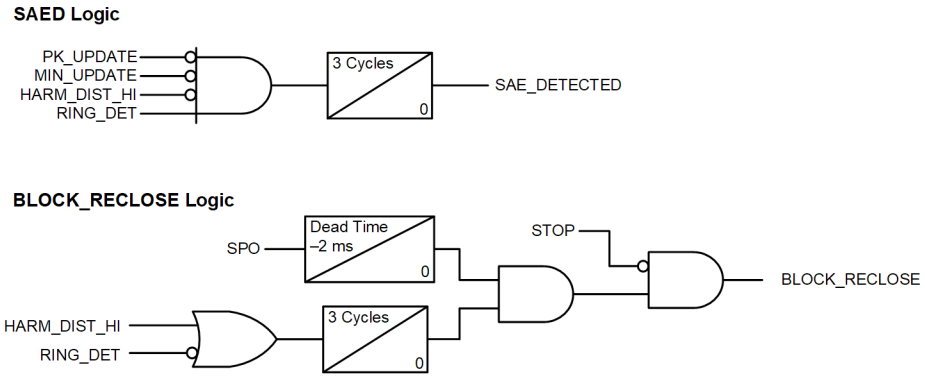

Fig. 14. Modified SAED and Block Reclose Logic When Shunt Reactors Are Present

3) System Source-to-Impedance Ratio (SIR) and Load Angle

We modeled ideal sources at each end of the transmission line and varied their source impedance independently to simulate different combinations of strong and weak, local and remote sources. Additionally, we varied the remote source angle between –30 degrees and 30 degrees to simulate various load flow levels in either direction.

4) Fault Parameters

We applied SLG faults at distances ranging from 10 percent to 90 percent along the transmission line. For transposed lines, faults were applied only on Phase A; for untransposed lines, faults were applied on all three phases. At each fault location, we applied both bolted and arcing faults. We varied the duration of the arcing faults to simulate faults that extinguish before the end of the dead time and others that do not.

B. Arc Model

We based the simulated arcing fault on the model developed by Johns, Aggarwal, and Song as described in [17] and [18]. A MATLAB System Object embedded in the Simulink model uses trapezoidal integration to solve the primary and SA conductance differential equations at each time step and its output controls a variable resistor in the fault path. The calculations are coordinated with the line breaker status to synchronize switching from the primary arcing state to the secondary arcing state. The fault model also calculates the arc length and restrike voltage at each time step in the secondary arcing state. The primary arc length (which is the initial condition for the secondary arcing state) can be varied to control the arc extinction time (i.e., to make the arc extinction time shorter or longer than the reclosing dead time). To simulate arc extinction and reignition during the secondary arcing state, an ideal switch in the fault path is opened at each current zero and reclosed when the calculated restrike voltage exceeds the measured arc voltage. The arc current is measured for control of the switch and to validate the arc model performance against previously published results.

C. Simulation Results

This section discusses the following:

- Behavior of the open-phase voltage angle for bolted faults and when no faults are present on the open phase
- Behavior of the open-phase voltage magnitude for uncompensated and compensated transmission lines
- Performance of the proposed algorithm for temporary and permanent faults on uncompensated and compensated transmission lines
- Details and results of comprehensive simulated test cases

1) Behavior of the Open-Phase Voltage Angle During and After Faults

Prior literature proposes using the open-phase voltage angle to determine if the SA has extinguished [10] [11]. References [10] and [11] assume that the open-phase voltage angle lags the angle of its unfaulted state by approximately 90 degrees when the fault is present and that it moves between the two healthy phase voltages, in the healthy voltage angle sector, after the fault is extinguished. This assumption is accurate if the line is transposed or if we consider only the ES coupling between the healthy phases and the open phases. The results in this section show that because of EM coupling, we cannot reliably use the angle of the open-phase voltage as an indication that the SA has extinguished.

We varied the line tower configuration, line loading, line length, SIR, and fault location to see how they affected the angle of the open-phase voltage during a bolted fault. The combination of tower configurations and line loading affected the open-phase voltage angle the most, so only those results are discussed.

Fig. 15 shows the open-phase voltage magnitude and angle for bolted faults on Phase A as we varied the line loading from –20 degrees to 20 degrees. These simulations were done on a 220 kV line with an SIR of 1 at both ends and a line length of 30 km. The figure shows that the angle of the open-phase voltage lies outside of the healthy voltage angle sector for reverse line loading (when the remote voltage has a positive angle) but enters the healthy voltage angle sector for forward line loading (when the remote voltage has a negative angle).

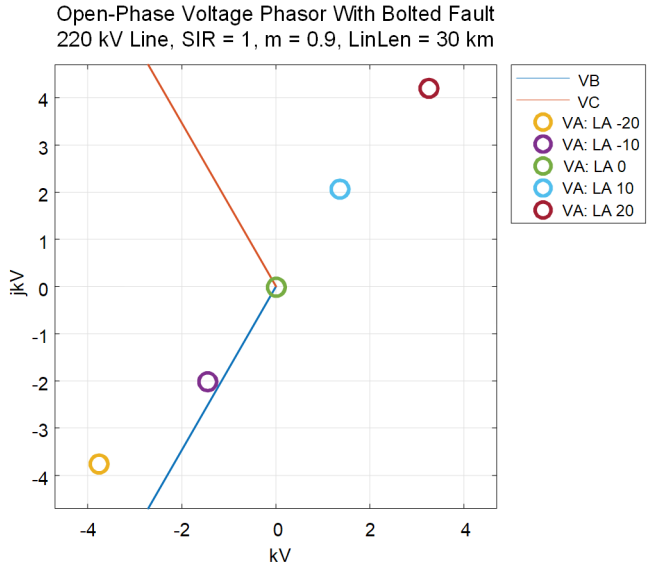

Fig. 15. VOpn Phasor for an Untransposed 30 km, 220 kV Line Under Various Loadings During a Bolted Fault

Recall that during a bolted fault, the ES component is negligible and VOpn contains mostly the EM component (see Subsection II.C). Furthermore, the Z_{AC} mutual impedance of this line is almost 20 percent greater than Z_{AB} because of the tower configuration. Therefore, the EM coupling in this configuration pulls the angle of the open-phase voltage closer to $Z_{AC} \bullet I_{CS}$ than to $Z_{AB} \bullet I_{BS}$, which causes the open-phase voltage to cross into the healthy voltage angle sector. This combination of an untransposed line and the load direction and magnitude shows how the VOpn angle may cross into the healthy voltage angle sector when a bolted fault is present on the open phase.

Fig. 16 shows the open-phase voltage of a 400 kV line with a length of 150 km, SIR of 0.1 at both ends of the line, and after the SA has extinguished. In this particular plot, Phase C is open and the remote voltage source angle was varied from –25 degrees to 25 degrees. Because of the horizontal tower configuration, Z_{BC} is about 23 percent greater than Z_{AC}. Therefore, the ES portion of the open-Phase-C voltage lies closer to Phase B. As the load angle increases in the positive direction, the open-phase voltage angle crosses Phase B after the SAE and is no longer inside the healthy phase voltage angle sector. This is due to a combination of unequal mutual coupling and heavy loading.

These results show the unreliability of using the open-phase voltage angle to determine if a fault is still present on a line.

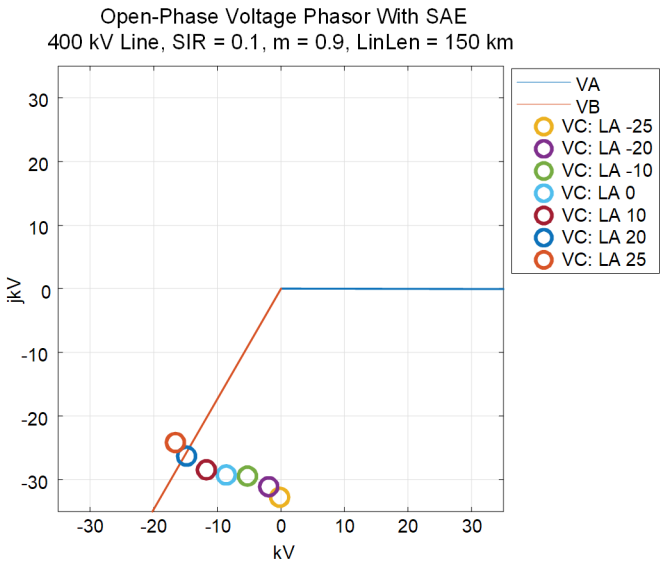

Fig. 16. VOpn Phasor for an Untransposed 150 km, 400 kV Line Under Various Loadings After SAE

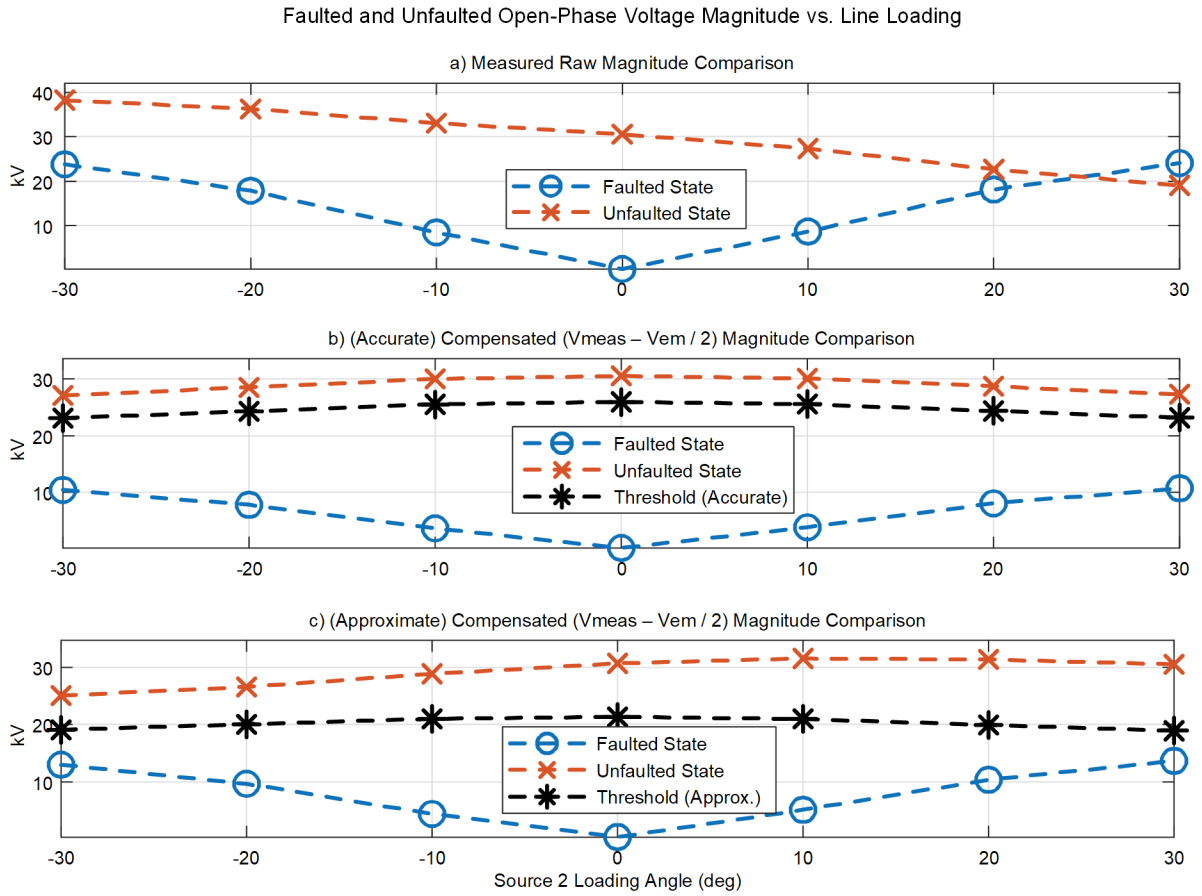

Fig. 17. Comparing Faulted and Unfaulted Open-Phase Voltage Magnitude for an Uncompensated Line

2) Open-Phase Voltage Magnitude for Uncompensated and Compensated Transmission Lines

We examined the open-phase voltage magnitude, |VOpn|, during a permanent bolted fault and after SAE, as shown in Fig. 17. The study involved an untransposed uncompensated 400 kV, 100 km line with an SIR of 0.1 at both ends. We varied the line loading from –30 degrees to 30 degrees and simulated the fault at 0.9 pu from the sending terminal.

Fig. 17a reveals that the |VOpn| during a bolted fault may exceed |VOpn| after the SAE, which can complicate SAE detection when using a magnitude check and threshold (see Subsection II.C for a description of this anomaly). As discussed in Subsection III.C.4, we solve this problem by subtracting half the total EM voltage from the measured open-phase voltage.

Fig. 17b shows the plots of accurately compensated open-phase voltage magnitudes by using the actual unique mutual impedances between the healthy phases and the open phase for the untransposed line, and Fig. 17c shows the approximately compensated open-phase voltage magnitudes by using an averaged mutual impedance value for the untransposed line. The figure shows a clear difference between the bolted (Faulted State) and SAE (Unfaulted State) voltage magnitudes in both compensated cases. Furthermore, a threshold obtained by taking 85 percent of the estimated ES voltage provides a good separation between the bolted fault and the SAE voltage magnitudes. When arcing is present, we rely on harmonics to block reclosing. Therefore, we did not perform the magnitude analysis while arcing was present.

Fig. 18 shows the open-phase voltage magnitude for a bolted fault at 0.9 pu from the sending end (Faulted State) and after SAE (Unfaulted State) for the transposed version of the same line but with 75 percent shunt-reactor compensation and reactors on both ends of the line. It can be seen that |VOpn| is highly variable and depends on the EM component (line loading) because the properly sized neutral reactor cancels the ES component, rendering a magnitude check unreliable.

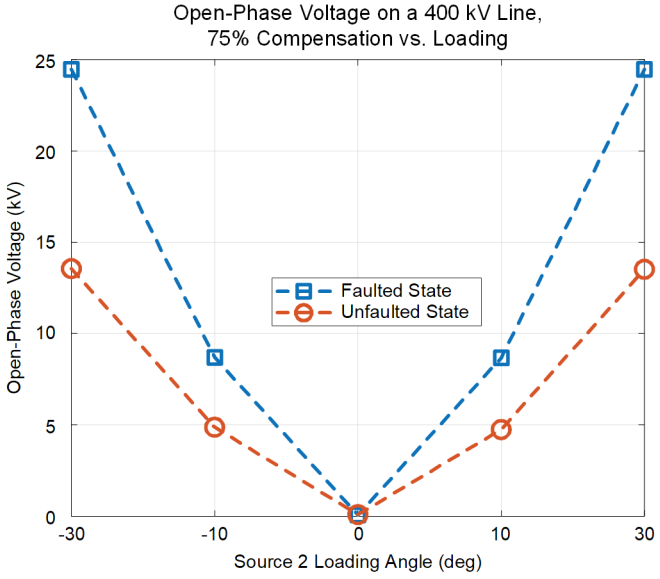

Fig. 18. Comparing Faulted and Unfaulted Open-Phase Voltage Magnitude on a 75% Compensated Transposed Line

Fig. 19 shows the open-phase voltage magnitude after SAE for each phase of the untransposed version of the same 75 percent compensated, 400 kV transmission line as in Fig. 18. The post-SAE voltage magnitude for the untransposed line is larger than for the transposed line and varies between phases. This is because of the imperfect nature of the switched reactor compensation (i.e., not all mutual admittances are canceled equally, and none are canceled perfectly). However, Fig. 19 shows that, as with the transposed case, the voltage magnitude after SAE can be smaller than the faulted state voltage magnitude, and it still consists mostly of the EM component. This demonstrates that even for untransposed lines, an alternative method to the open-phase voltage magnitude check is still required for accurate SAE detection.

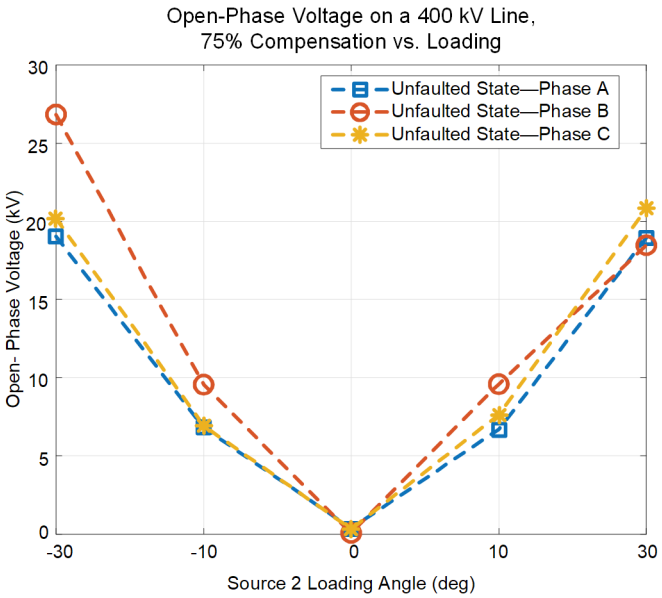

Fig. 19. Comparing Unfaulted Open-Phase Voltage Magnitudes on a 75% Compensated Untransposed Line

3) Performance of the Proposed Algorithm for an Uncompensated Transmission Line

This section analyzes the performance of the proposed algorithm in detecting permanent faults and detecting SAE before the expiration of the dead time in an uncompensated transmission line. We consider a 100 km, 400 kV untransposed line with an SIR of 0.1 at both ends of the line. A significant reverse line loading is simulated by keeping the remote source voltage leading the local source voltage by 20 degrees.

a) Permanent Fault

A permanent Phase A SLG fault at a fault location of 0.1 pu occurs at around 0.35 s and the Phase A breaker opens at around 0.45 s. Fig. 20 shows the raw voltage and current of the faulted phase.

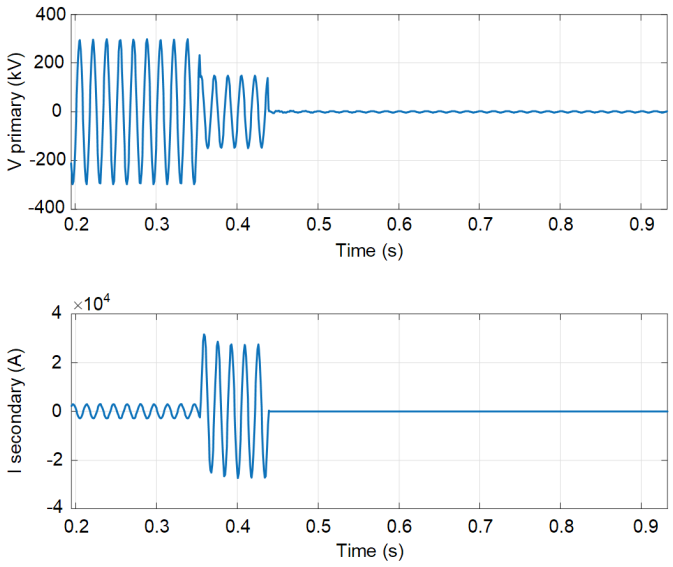

Fig. 20. Faulted-Phase Raw Voltage and Current for a Permanent Fault in an Uncompensated Line

A dead time of 0.5 s is assumed (the breaker reclosing is not simulated). Fig. 21 shows the algorithm performance. The top part of the figure shows the faulted-phase voltage in primary kilovolts and the derived analogs used in the algorithm. The plot is zoomed in to show the various quantities clearly. The quantities shown are as follows:

- **Mag** = low-pass filtered phasor magnitude (VOpn_Mag_LP)
- **Min** = minimum-tracked value of Mag
- **Pk** = peak-tracked value of Mag
- **Mag_Comp** = compensated Mag, $VOpn_{Comp}$ (see Subsection III.C.4)
- **Thresh** = Mag_Check_Thresh (see Subsection III.C.4)

The trace for Mag is barely visible because it is behind the traces of Min and Pk.

The middle part of Fig. 21 shows the following quantities:

- **Harm_Dist** = The rms sum of the second through fifth harmonics
- **Thresh** = The harmonic high threshold (5 percent of VOpn_Mag_LP)

The bottom part of the figure shows the algorithm outputs. The RUN output, triggered by the SPO bit, arms the algorithm. The close-in bolted permanent fault causes the open-phase voltage to remain low. The lack of signal changes after 0.5 s causes PK_UPDATE and MIN_UPDATE to deassert quickly. The voltage seen is mostly due to EM coupling from the other two healthy phases and corresponds to 0.1 pu of the total EM voltage (see (4)). The compensated magnitude is well below the magnitude threshold (dashed black trace in top plot), indicating that the fault still exists on the line. Therefore, the MAG_OK bit remains deasserted. The harmonics are very low, as is expected for a bolted fault, which causes the HARM_DIST_HI bit to deassert. The SAE_DETECTED bit does not assert because MAG_OK does not assert. MAG_OK being deasserted for 3 cycles prior to the dead time expiring causes BLOCK_RECLOSE to assert, which can be used to block reclosing.

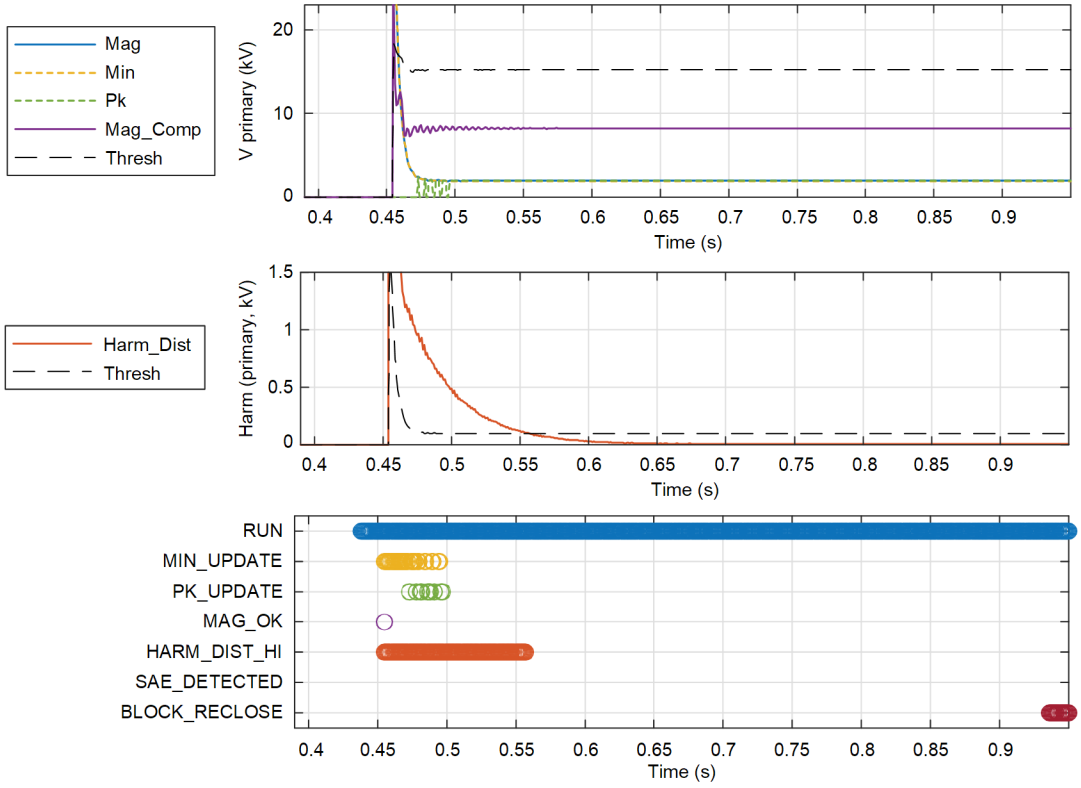

Fig. 21. Algorithm Performance for a Permanent Fault in an Uncompensated Line

b) Temporary Fault With a Secondary Arc

We simulated a temporary fault at the same fault location and for the same system as in the previous case. The arc extinction took about 300 ms. Fig. 22 shows the raw waveforms.

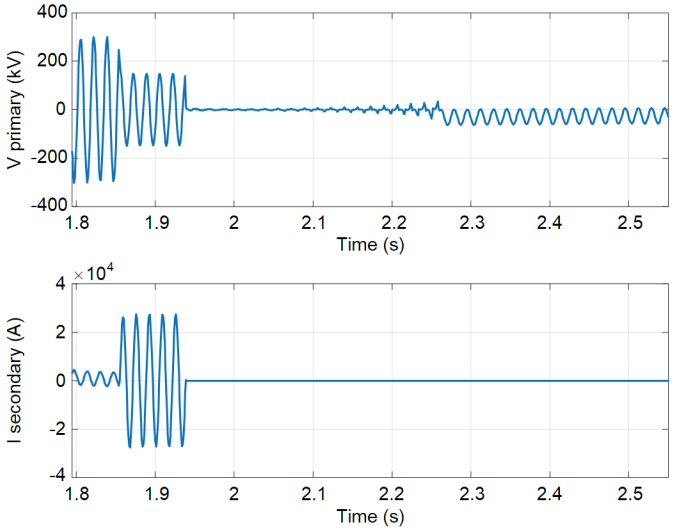

Fig. 22. Faulted-Phase Raw Voltage and Current for a Temporary Fault in an Uncompensated Line

Fig. 23 shows the algorithm performance. As the arc length increases during secondary arcing, Mag keeps increasing until arc extinction, as indicated by a regular assertion of PK_UPDATE until arc extinction, when the voltage magnitude stabilizes. The loading direction is such that the EM component cancels a portion of the ES voltage, leading to a lower Mag. The compensated magnitude, Mag_Comp, removes this opposing EM part and thus recovers the higher ES part, which results in MAG_OK asserting after arc extinction. The harmonic distortion is high during the arcing period and drops to almost zero after arc extinction, at which point HARM_DIST_HI deasserts. Three cycles after all the checks are passed (i.e., there are no new peak and minimum values, no significant harmonic distortion, and the compensated magnitude is above the threshold), SAE is declared by asserting SAE_DETECTED, which can be used for reclosing supervision or for faster reclosing.

4) Performance of the Proposed Algorithm for a Compensated Transmission Line

This section analyzes the performance of the proposed algorithm for detecting permanent faults and SAE before the dead-time expiration in a shunt-reactor-compensated transmission line. We used a 100 km, 400 kV transposed transmission line with two four-legged reactor banks connected on both ends of the line to compensate 75 percent of the line. The line is connected to strong sources with an SIR of 0.1 at both ends of the line and the line loading is kept at 15 degrees in the forward direction (i.e., from the sending end to the remote end). We simulated the fault at 0.9 pu distance from the local relay and set the dead time for reclosing to 0.5 s.

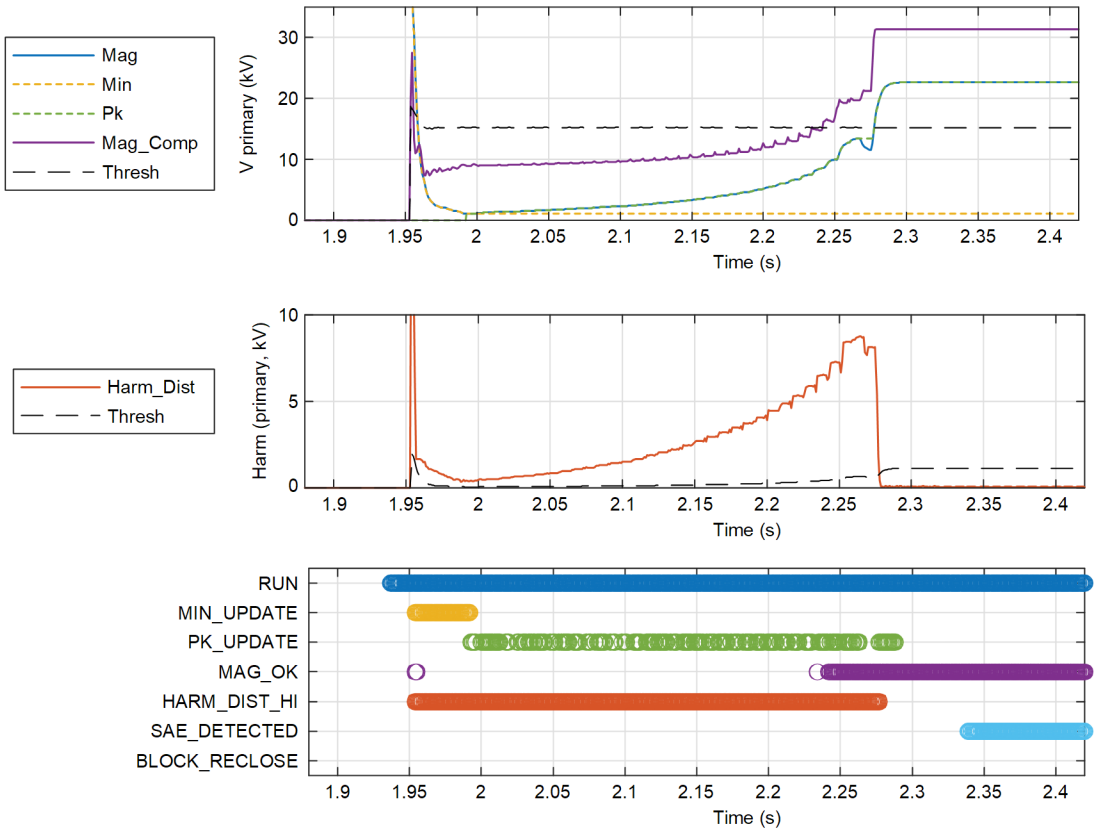

Fig. 23. Algorithm Performance for a Temporary Fault in an Uncompensated Line

a) Permanent Fault

A permanent Phase A SLG fault occurs at around 0.08 s and the Phase A breaker opens at around 0.17 s. Fig. 24 shows the raw voltage and current of the faulted phase.

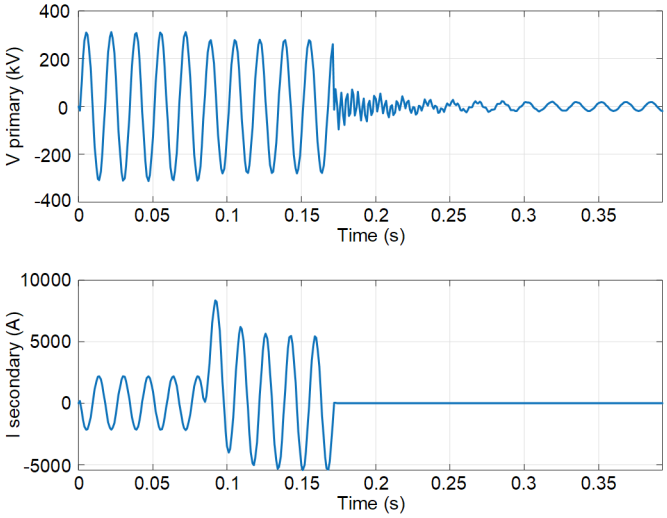

Fig. 24. Faulted-Phase Raw Voltage and Current for a Permanent Fault in a Compensated Line

Fig. 25 shows the algorithm performance. The top part of the figure includes a mean value, Mean (see Subsection III.D.5), and does not contain the compensated magnitude or the magnitude threshold because those are not calculated by the algorithm for a shunt-reactor-compensated line. The bottom part of the figure contains the RING_DET output instead of a MAG_OK bit because ringing detection is used to detect SAE when shunt reactors are present.

Because this is a bolted fault, the magnitude settles down quickly to a low value, thereby deasserting PK_UPDATE and MIN_UPDATE. The harmonics are very low, as is expected for a bolted fault, which causes the HARM_DIST_HI bit to deassert. The SAE_DETECTED bit does not assert because ringing in the voltage is not detected. Two milliseconds before the dead-time expiration, the BLOCK_RECLOSE bit asserts, which can be used to block reclosing.

b) Temporary Fault With a Secondary Arc

We simulated a temporary fault at the same fault location and for the same system as in the previous section. Fig. 26 shows the raw waveforms. After the breaker opens, secondary arcing starts and extinguishes almost immediately (after about 20 ms). This is evident from the ringing in the raw voltage waveform. Compare this to the arc extinction time in the uncompensated line, which was about 300 ms. This observation highlights the importance of a properly sized neutral reactor for rapid extinction of a secondary arc.

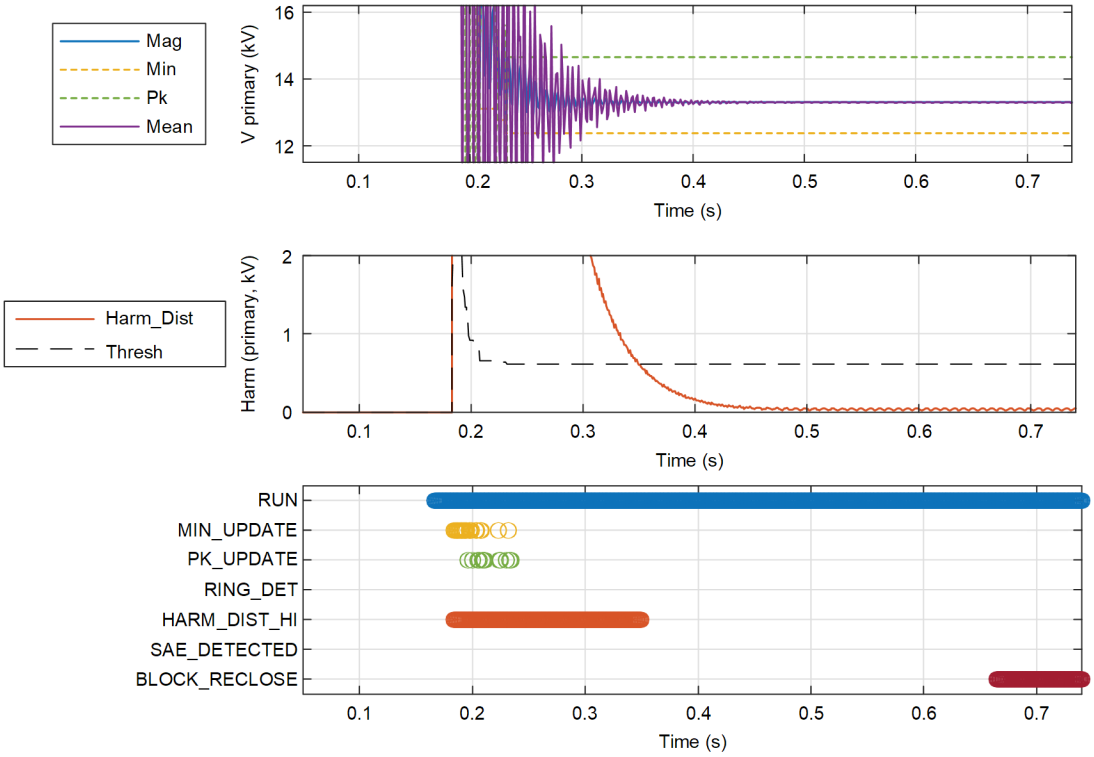

Fig. 25. Algorithm Performance for a Permanent Fault in a Compensated Line

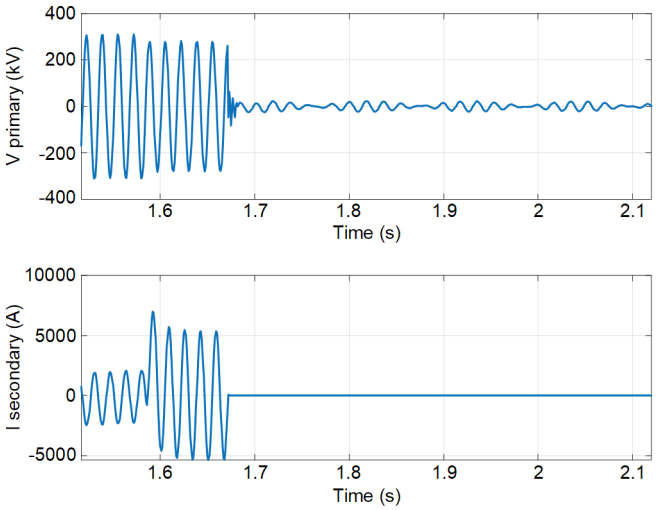

Fig. 26. Faulted-Phase Raw Voltage and Current for a Temporary Fault in a Compensated Line

Fig. 27 shows the algorithm performance. Mag shows the classic beat frequency oscillation when the arc extinguishes and ringing starts. The Pk and Min values stabilize after about half a cycle of the beat frequency, thereby deasserting PK_UPDATE and MIN_UPDATE. In the middle plot, adaptive updating of the harmonic threshold can be seen once the mean value stabilizes. At this point, the threshold for harmonic distortion switches from 5 percent of V_{MIN} to 5 percent of V_{MEAN} (purple trace in top plot) plus an adaptive component (i.e., LkgFact • V_{RING}, see (22)). The adaptive component of the threshold decreases as the ringing decays. The ringing asserts the RING_DET bit, which then latches until the breaker is reclosed. Three cycles after all the checks are passed (i.e., there are no new peak or minimum values, no significant harmonic distortion, and ringing is detected), SAE is declared by asserting SAE_DETECTED, which can be used for reclosing supervision or faster reclosing.

5) *Comprehensive Test Cases*

We tested the algorithm extensively for each of the line configurations—uncompensated transposed, uncompensated untransposed, compensated transposed, and compensated untransposed—against a number of changing parameters including voltage levels, tower configurations, line lengths, fault locations, source impedance ratios, phases, percentage compensations, and reactor switching statuses. Table I in Appendix E shows the list of variables changed and the range of values for each case. Some combinations of parameters could not be run due to unrealistic load flow. However, the algorithm worked as expected for the test cases that did run successfully.

V. Field Events, Algorithm Performance, and Discussion

In this section we analyze the performance of the proposed algorithm for four different field events. The first event is a classic arc extinction within the reclosing dead time on an uncompensated line. The second event is an arc extinction on a shunt-reactor-compensated line. The third event is a permanent fault on a compensated line. Finally, the fourth event is an arc extinction on a compensated line with downward ringing behavior.

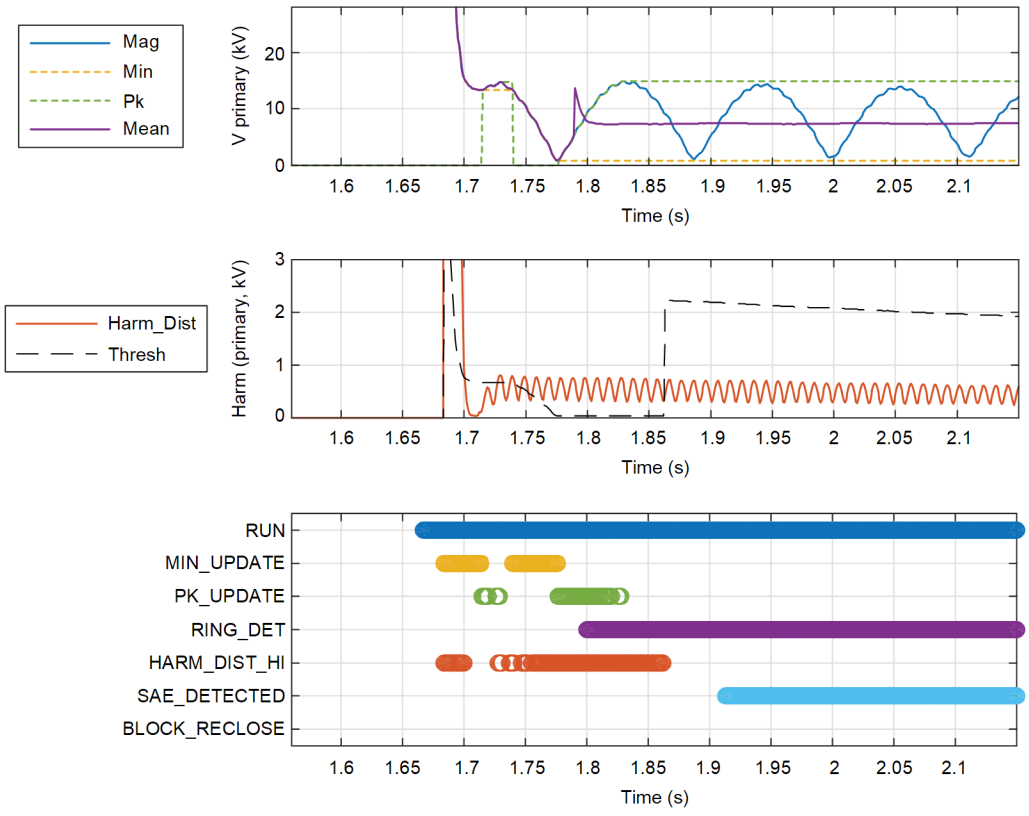

Fig. 27. Algorithm Performance for a Temporary Fault in a Compensated Line

For each event, we extracted raw currents and voltages from COMTRADE files collected from relays protecting the line. Further, We preprocessed the raw voltages to resample them to the algorithm processing rate, track the fundamental frequency, and calculate the voltage phasors at the fundamental and second through fifth harmonics. We also preprocessed the raw currents to calculate the fundamental frequency phasors for the unfaulted phases. We then fed these values into the algorithm to validate its performance.

A. Field Event 1—Classic Secondary Arc Extinction on an Uncompensated Transposed Parallel Line

This event is a Phase-B-to-ground fault on a 60 Hz, 230 kV, 162.4 km parallel line without shunt-reactor compensation. The relay reported the fault location as 30.3 km. This is the same event shown in Fig. 7.

Fig. 28 shows the raw Phase-B voltage and current. The fault occurs 0.087 s into the event and the faulted phase is isolated at 0.138 s. After isolation, there is a short period of high-frequency voltage transients followed by a longer period of lower-frequency distortion indicative of the presence of secondary arcing that persists until about 0.45 s. At 0.67 s, the open phase is successfully re-energized from the remote end, and at 0.891 s, the local breaker closes and current starts to flow.

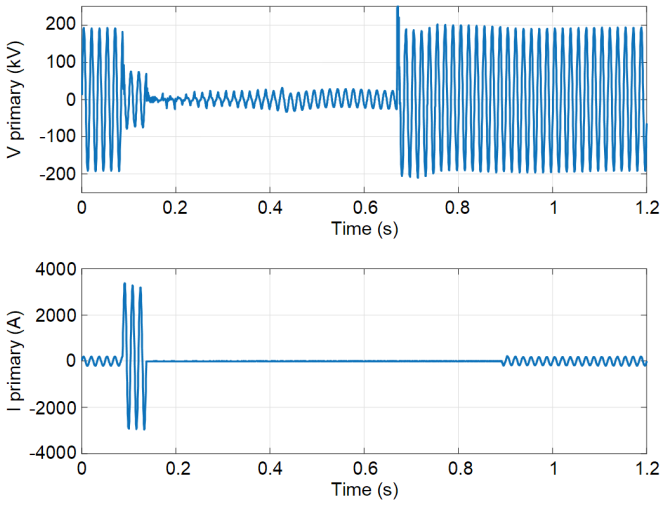

Fig. 28. Field Event 1—Raw Phase-B Voltage and Current

The local relay settings indicate a dead time of 34 cycles (0.567 s at 60 Hz). The remote relay settings are not available, but based on the timing of the line re-energization, we assume a 30-cycle dead-time setting (0.5 s at 60 Hz).

The voltage angles, referenced to positive-sequence, are shown in Fig. 29. During the period of secondary arcing, the Phase-B voltage angle (red trace) rotates clockwise toward the Phase-C voltage angle (yellow trace). However, after the arc extinguishes, the Phase-B voltage angle remains outside the region between the Phase-A (blue trace) and Phase-C voltage angles. This behavior indicates that the open-phase voltage angle is not a reliable signal for detecting arc extinction for this case.

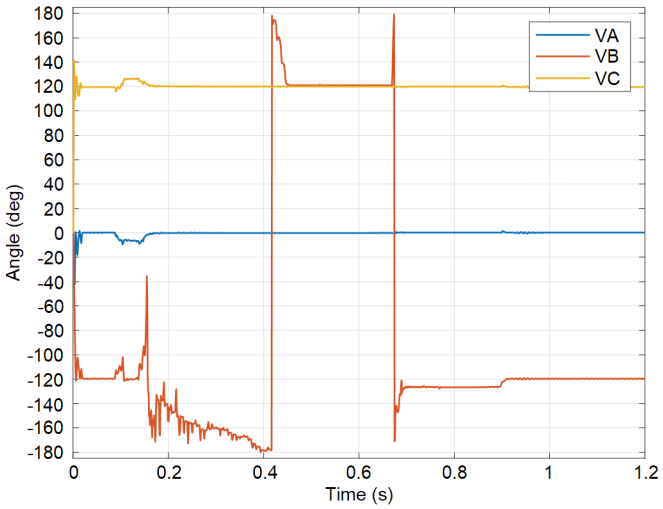

Fig. 29. Field Event 1—Voltage Angles

Fig. 30 shows the algorithm response. Refer to Subsection IV.C.3.a for a description of signals used in the figure.

For this case, the currents and voltages from the parallel line and the line parameters, including the mutual impedances and admittances between the parallel lines, are not available. Therefore, the algorithm is not able to calculate the compensated magnitude or the adaptive threshold Mag_Check_Thresh (see (21)). Instead, a static magnitude threshold of 10 percent of the nominal line-to-neutral voltage is used for the algorithm. As discussed in Subsection IV.C.2, the compensated voltage magnitude and adaptive threshold are required to account for the influence of the EM coupling from the unfaulted phases for all system conditions. However, simulation results indicate that 10 percent is a reasonable approximation for lines that are shorter than 300 km and which are not heavily loaded.

Shortly after the faulted phase is isolated, the minimum tracker (yellow trace) stops updating (MIN_UPDATE does not assert for the remainder of the event) and PK_UPDATE asserts intermittently as new peaks are found until the open-phase voltage magnitude stops increasing at around 0.45 s. The compensated voltage magnitude Mag_Comp (purple trace) follows Mag and stabilizes above the 10 percent threshold, at which point MAG_OK asserts and remains asserted. This is the expected behavior because the SA lengthens and its resistance increases until the arc extinguishes and the voltage magnitude stabilizes.

The red trace in the middle plot shows the calculated harmonic distortion, Harm_Dist (see (16)). It is highly elevated during the period of high-frequency transients after isolation and then starts to decrease. HARM_DIST_HI asserts immediately with the assertion of RUN until around 0.45 s, when Harm_Dist drops below the threshold and HARM_DIST_HI deasserts.

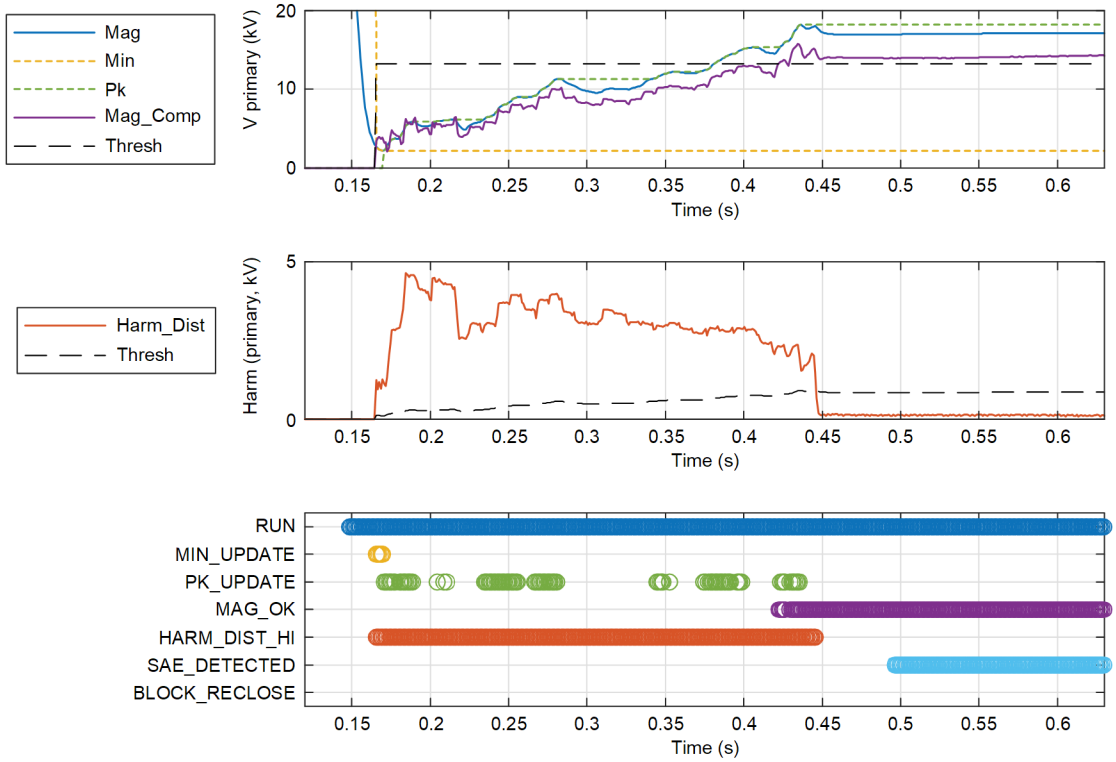

Fig. 30. Field Event 1—Algorithm Response

Three cycles after HARM_DIST_HI deasserts (slightly before 0.5 s), SAE_DETECTED asserts. This can be used as confirmation that the fault is no longer present for reclosure supervision at the end of the dead time. Alternatively, the assertion of SAE_DETECTED could be used to initiate reclosing before the end of the dead time. In this event, the line was successfully re-energized at 0.67 s (at the end of the fixed dead time). Had the assertion of SAE_DETECTED been included in the reclosing logic, reclosing could have been attempted approximately 0.15 s sooner, subject to the breaker minimum duty cycle time.

B. Field Event 2—Secondary Arc Extinction on a Compensated Transposed Parallel Line

This event is a Phase-A-to-ground fault on a 60 Hz, 230 kV, 145 km parallel line with shunt-reactor compensation on one end of the line. The relay reported the fault location as 96.76 km. This is the same event shown in Fig. 12.

Fig. 31 shows the raw Phase-A voltage and current. The fault occurs 0.486 s into the event and the faulted phase is isolated at 0.554 s. After isolation, there is a short period of high-frequency voltage transients followed by a longer period of ringing with decreasing amplitude that persists until about 1.079 s, when the open phase is successfully re-energized from the remote end. At 1.257 s, the local breaker closes and current starts to flow.

The local relay settings do not have the reclosing function enabled, so we assume that separate breaker relays are used for reclosing. Based on the timing of the line re-energization, we assume a 30-cycle dead-time setting (0.500 s at 60 Hz). The size of the shunt reactor is not known, but inspection of the open-phase voltage indicates a ringing frequency of about 49 Hz (i.e., a beat frequency of about 11 Hz in the open-phase voltage magnitude), which corresponds to a phase compensation of about 67 percent (refer to Subsection III.D.1 for further details regarding this calculation). Furthermore, the SA extinguishes in less than 0.1 s, so we assume that the neutral reactor is appropriately sized as described in Appendix B.

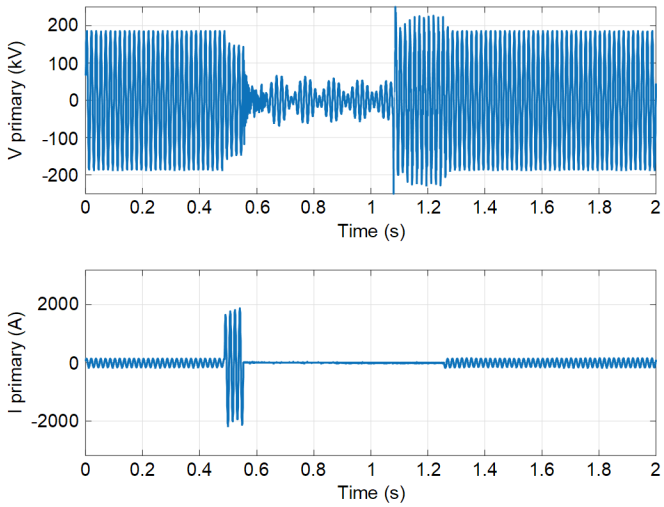

Fig. 31. Field Event 2—Raw Phase-A Voltage and Current

The voltage angles, referenced to positive-sequence, are shown in Fig. 32. During the short period of secondary arcing, the Phase-A voltage angle (blue trace) rotates counter-clockwise toward the Phase-C voltage angle (yellow trace). The appearance of large oscillations in the plot is due to the Phase-A voltage angle sign changing by nearly 180 degrees. After the arc extinguishes, the Phase-A voltage angle oscillates with a

mean value of approximately its pre-fault angle. The mean value of the angle does not change from its pre-fault value because there is stronger coupling from the parallel line Phase-A conductor than from other healthy phase conductors. This causes the Phase-A voltage angle to remain well outside the region between the Phase-B (red trace) and Phase-C voltage angles. As with Field Event 1, this behavior indicates that the open-phase voltage angle is not a reliable signal for detecting arc extinction.

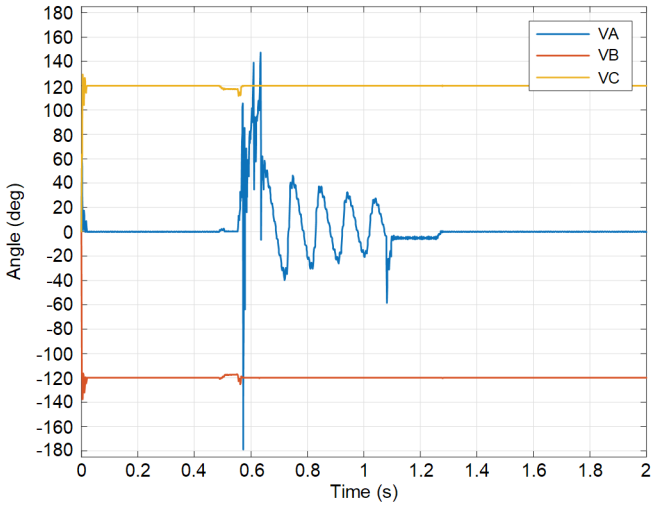

Fig. 32. Field Event 2—Voltage Angles

Fig. 33 shows the algorithm response. Refer to Subsection IV.C.4.a for a description of signals used in the figure.

After the faulted phase is isolated, Mag displays oscillations with a downward trend for about 0.056 s due to the high-frequency transients. At 0.639 s, the voltage magnitude stops decreasing (MIN_UPDATE deasserts and remains deasserted for the remainder of the event) and the peak tracker starts tracking the upward movement of the open-phase voltage magnitude. PK_UPDATE asserts until the open-phase voltage magnitude stops increasing at around 0.689 s. Mean tracks Mag until ringing is detected (RING_DET asserts), at which point the averager filter removes the beat frequency oscillations and Mean tracks the fundamental frequency component of the open-phase voltage magnitude.

Harm_Dist (red trace in the middle plot) is highly elevated during the period of high-frequency transients and then decreases during the period when the peak tracker is updating. HARM_DIST_HI asserts immediately with the assertion of RUN. Shortly after the peak tracker stops updating, RING_DET asserts. Approximately one beat frequency period later, the threshold for the Harm_Dist comparison switches from 5 percent of V_{MIN} to 5 percent of V_{MEAN} plus an adaptive component (LkgFact • V_{RING}, see (22)), as is evident from a step increase in Thresh. The new threshold keeps HARM_DIST_HI deasserted for the remainder of the event even though Harm_Dist exhibits a ripple with peaks above the static threshold of 5 percent of Mag.

Three cycles after RING_DET asserts, at around 0.8 s, SAE_DETECTED asserts. In this event, the line was successfully re-energized at 1.079 s (at the end of the fixed dead time). Had the assertion of SAE_DETECTED been included in the reclosing logic, reclosing could have been attempted approximately 0.325 s sooner, subject to the breaker minimum duty cycle time.

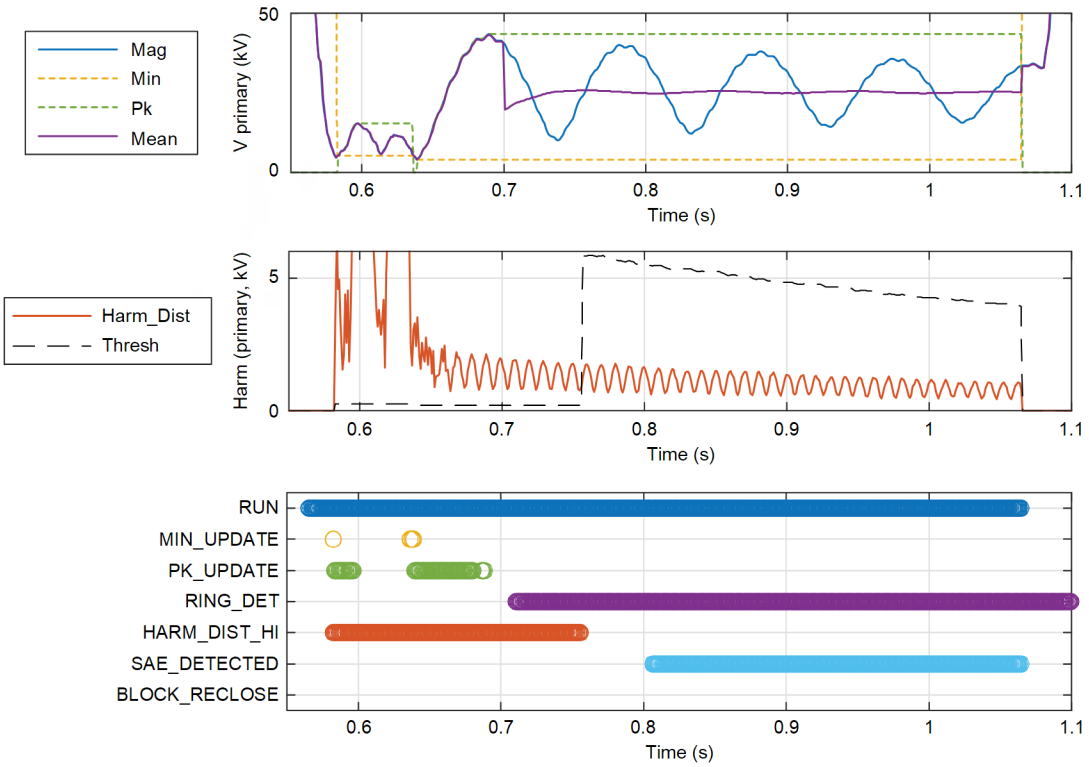

Fig. 33. Field Event 2—Algorithm Response

C. *Field Event 3—Permanent Fault on a Compensated Transposed Parallel Line*

This event is a Phase-B-to-ground fault on the same line described in Field Event 2. The relay reported the fault location as 56.82 km.

Fig. 34 shows the raw Phase-B voltage and current. The fault occurs 0.491 s into the event and the faulted phase is isolated at 0.55 s. After isolation, there is a short period of high-frequency voltage transients followed by a longer period of low amplitude with little distortion and no discernible ringing. An unsuccessful reclosing attempt is made from the remote end at 1.088 s.

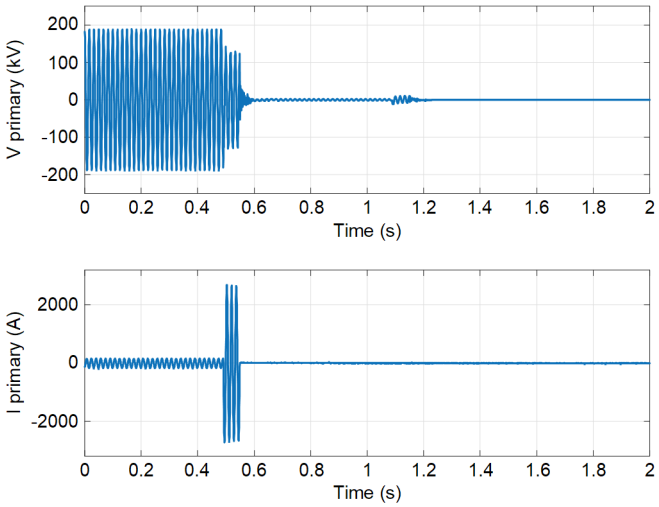

Fig. 34. Field Event 3—Raw Phase-B Voltage and Current

The voltage angles, referenced to positive-sequence, are shown in Fig. 35. During the fault, the Phase-B voltage angle (red trace) rotates counter-clockwise toward the Phase-A voltage angle (blue trace) but does not enter the region between the Phase-A and Phase-C (yellow trace) voltage angles for any significant period of time.

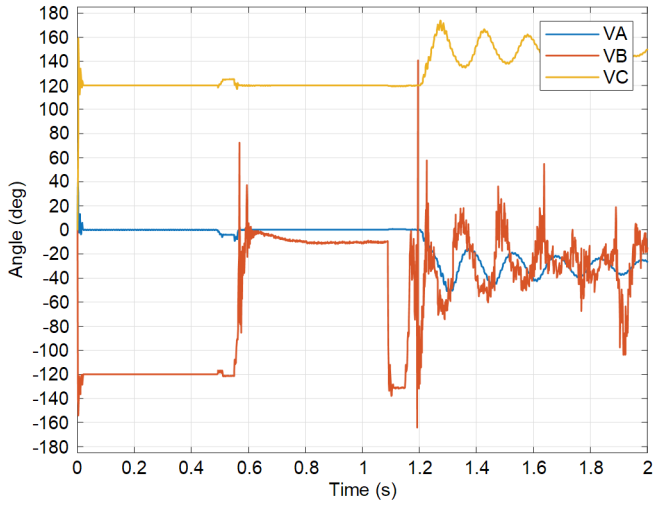

Fig. 35. Field Event 3—Voltage Angles

Fig. 36 shows the algorithm response. Because ringing is not detected for this event (RING_DET remains deasserted for the entire event), the mean value of the open-phase voltage magnitude, Mean (purple trace), tracks Mag and plots on top of it. After the faulted phase is isolated, the voltage magnitude is very low (less than 1 V secondary) and displays small oscillations for about 0.045 s, after which it remains relatively flat with only a slight camber. During the oscillatory period, the minimum tracker (yellow trace) updates intermittently (MIN_UPDATE asserts) and the peak tracker (green trace) is reset with each new minimum so that it does not latch onto an incorrect value. At 0.648 s, the voltage magnitude stops decreasing (MIN_UPDATE deasserts and remains deasserted for the remainder of the event) and the peak tracker starts tracking the slight upward movement of the open-phase voltage magnitude. PK_UPDATE asserts intermittently until 0.712 s.

Harm_Dist is elevated during the oscillatory period and then stabilizes around the threshold. HARM_DIST_HI asserts intermittently throughout the entire event. Because ringing is not detected, the threshold remains at 5 percent of V_{MIN} throughout the event.

Because RING_DET does not assert and HARM_DIST_HI asserts throughout the event, two processing intervals before the expiration of the dead time, BLOCK_RECLOSE asserts, indicating that the fault is still present. This assertion can be used to block reclosing and convert to a three-pole trip.

D. *Field Event 4—Secondary Arc Extinction With Downward Ringing on a Compensated Transposed Line*

This event is a Phase-B-to-ground fault on a 60 Hz, 400 kV, 252 km line with shunt-reactor compensation on one end of the line. The relay reported the fault location as 176.52 km.

Fig. 37 shows the raw Phase-B voltage and current. The fault occurs 0.984 s into the event and the faulted phase is isolated at 1.035 s. After isolation, there is a short period of high-frequency voltage transients followed by a longer period of ringing with decreasing amplitude that persists until about 1.7 s, when the open phase is successfully re-energized from the local end. At 1.94 s, the remote breaker closes and current starts to flow. Note that the ringing is very sinusoidal in nature, unlike in previous events where the presence of two frequencies—lower ringing frequency and higher fundamental frequency—was evident.

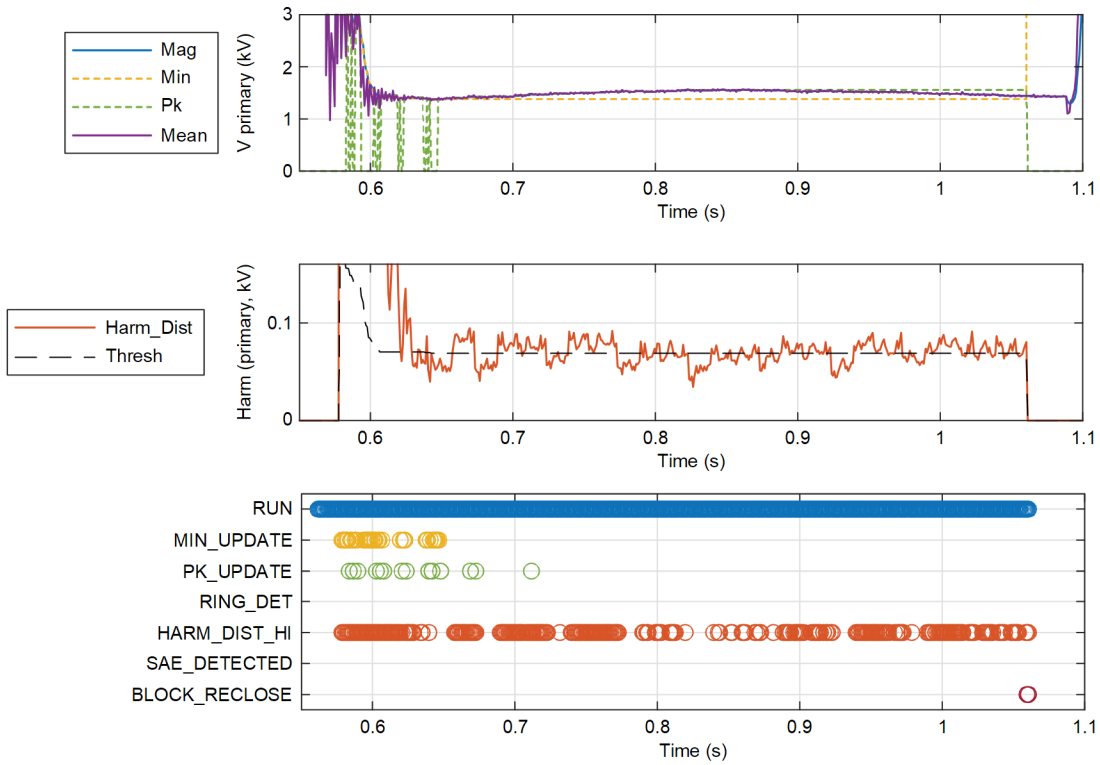

Fig. 36. Field Event 3—Algorithm Response

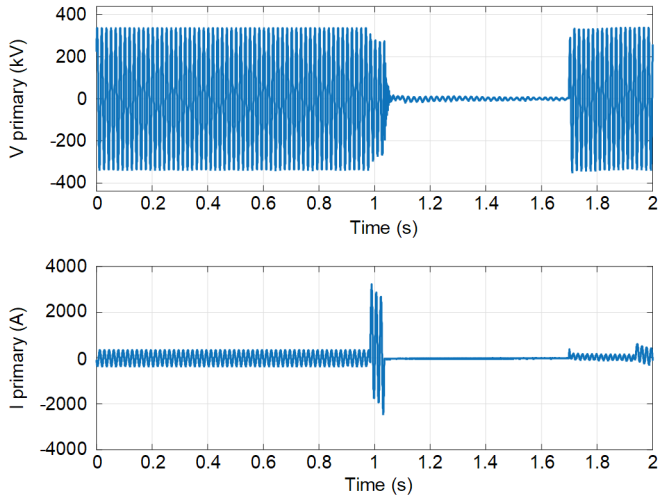

Fig. 37. Field Event 4—Raw Phase-B Voltage and Current

The local relay settings do not have the reclosing function enabled, so we assume that separate breaker relays are used for reclosing. Based on the timing of the line re-energization, we assume a 30-cycle dead-time setting (0.5 s at 60 Hz). The size of the shunt reactor is not known, but inspection of the open-phase voltage indicates a ringing frequency of about 50.97 Hz (i.e., a beat frequency of about 9 Hz in the open-phase voltage magnitude), which corresponds to a phase compensation of about 72 percent (see Subsection III.D.1 for more information). Furthermore, the SA extinguishes in about 0.04 s, so we assume that the neutral reactor is appropriately sized as described in Appendix B.

The voltage angles, referenced to positive-sequence, are shown in Fig. 38. During the short period of secondary arcing, the Phase-B voltage angle (red trace) rotates counter-clockwise toward the Phase-A voltage angle (blue trace). After the arc extinguishes, the Phase-B voltage angle oscillates continuously, covering all angles from –180 degrees to 180 degrees several times. This oscillation is due to the fact that the ringing signal consists of almost pure ringing frequency and very little fundamental frequency component. As with previous field events, this behavior indicates that the open-phase voltage angle is not a reliable signal for detecting arc extinction.

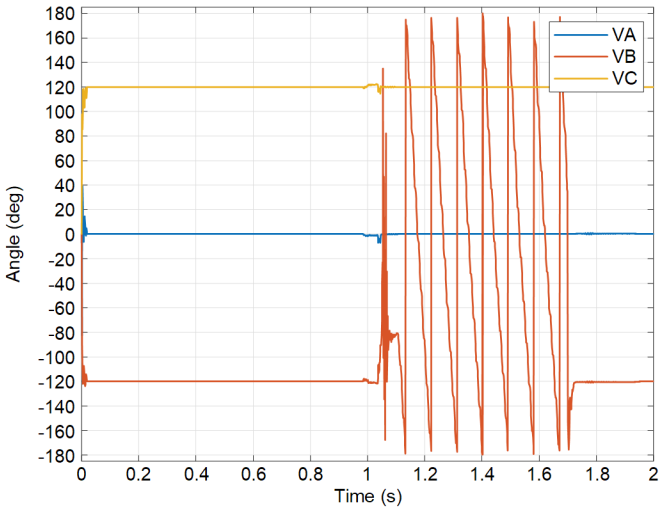

Fig. 38. Field Event 4—Voltage Angles

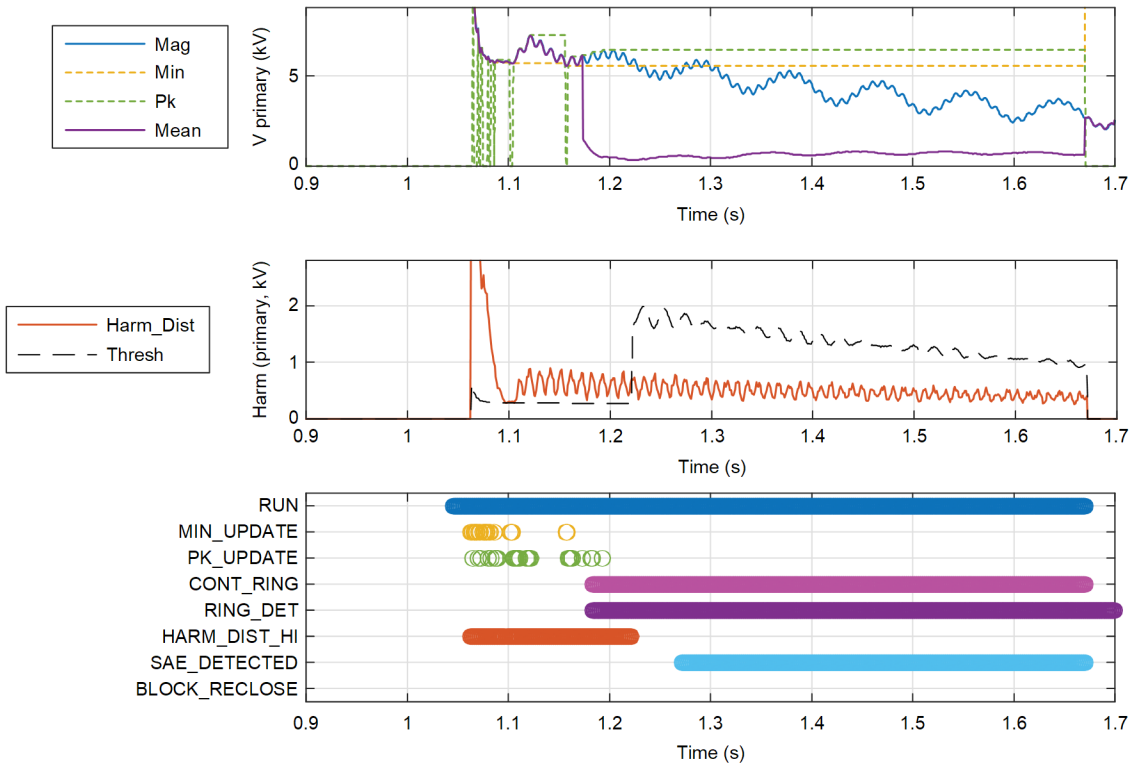

Fig. 39. Field Event 4—Algorithm Response

Fig. 39 shows the algorithm response. In the top plot, it can be seen that Mag (blue trace) continues to decrease even after ringing is detected. This is because it mostly contains the ringing component of the voltage as it leaks through the fundamental frequency phasor filter. The low value of fundamental frequency component is evident from the Mean plot (purple trace). Because the ringing decays with time, the consequent leakage into Mag also decays with time. However, the minima tracker (yellow trace) does not update even though new minimum values are found intermittently. This is because the minima tracker is paused by continuous ringing detection (CONT_RING in the bottom plot; see Subsection III.D.4). At 1.16 s, MIN_UPDATE deasserts and shortly after, PK_UPDATE deasserts when ringing begins (i.e., when RING_DET asserts). As shown in the middle plot, the assertion of RING_DET triggers adaptive updating of the harmonic threshold, which gets a boost to account for ringing leakage in harmonics. This results in the deassertion of HARM_DIST_HI at about 1.23 s. Three cycles after that, at about 1.27 s, SAE_DETECTED asserts, confirming that the fault is no longer present for reclosure supervision at the end of the dead time. Alternatively, the assertion of SAE_DETECTED could be used to initiate reclosing before the end of the dead time. In this event, the line was successfully re-energized at 1.7 s (at the end of the fixed dead time). Had the assertion of SAE_DETECTED been included in the reclosing logic, reclosing could have been attempted approximately 0.43 s sooner, subject to the breaker minimum duty cycle time.

VI. Conclusion

Single-pole tripping is used to clear temporary SLG faults while maintaining system stability. Typically, a fixed dead time is used for reclosing after a single-pole trip. However, in the single-pole-open state, an SA can be sustained through electrostatic (ES) and electromagnetic (EM) coupling to the two energized phases and the timing of the SAE can vary. An adaptive reclosing scheme that dynamically modifies the dead time could improve system stability by reclosing faster when the open phase does not have a fault and delaying or blocking reclosing when the open phase remains faulted. The critical part of any such scheme is an accurate open-phase fault detection method.

In the single-pole-open state, the line PT on the open phase provides the only direct measurement for detecting a fault. In this paper, we present an analytical and empirical assessment of the open-phase voltage to determine which characteristics are reliable for fault detection or SAE detection. These include the harmonic distortion, voltage magnitude, and ringing frequency. We then develop an algorithm based on these characteristics. All the reliable characteristics are considered to cover all system scenarios. The algorithm comprises two main parts: conditioning the measured voltage to extract the reliable signals and the logic to create binary outputs that can be used in a reclosing scheme.

Conditioning the measured voltage and choosing the correct signals for the system configuration are critical for avoiding incorrect fault-detection assessments. Significant harmonic distortion can indicate the presence of a fault, but ringing after SAE on shunt-reactor-compensated lines will also create harmonics in the voltage. Therefore, an adaptive harmonic

detection algorithm is employed for compensated lines in which 5 percent of the minimum-tracked value is used as a sensitive threshold until ringing is detected. When ringing is detected, the threshold is changed to 5 percent of the mean value of the fundamental frequency voltage magnitude plus an adaptive component proportional to the magnitude of the ringing frequency component of the voltage and a combined leakage factor dependent on the ringing frequency. For uncompensated lines, the fundamental voltage magnitude can be used directly as the base and a static 5 percent threshold is sufficient.

Additionally, for both compensated and uncompensated lines, upward movement in the open-phase voltage magnitude can indicate the presence of a fault. However, some faults may not create significant voltage harmonics or movement in the voltage magnitude. Therefore, it is not sufficient to say that the absence of these characteristics indicates that the open phase is unfaulted, and additional SAE signals are required. On uncompensated lines, the expected post-fault recovery voltage magnitude can be used for arc extinction detection, but the assessment must consider the EM coupling from the healthy phases. Therefore, the algorithm uses a compensated voltage magnitude with a portion of the EM coupling removed (based on line parameters and measured current in the healthy phases) and a dynamic threshold based on the ES coupling from the measured healthy phase voltages. On compensated lines, the mutual impedances of the shunt reactor cancel some percentage of the mutual admittances. This can lead to a very low post-fault recovery voltage, which cannot be distinguished from a fault condition. Therefore, the open-phase voltage magnitude is not a reliable SAE signal for compensated lines. Instead, the algorithm detects post-fault ringing.

Once the reliable signals are extracted, they are combined in simple logic to provide binary outputs that can be used to control automatic reclosing. When neither of the fault detection signals (high harmonics and voltage magnitude movement) are present and the SAE signal (i.e., a magnitude check for uncompensated lines and ringing detection for compensated lines) is present for a configurable minimum amount of time, e.g., 3 cycles, the SAE_DETECTED output is asserted. This output can be used as confirmation to permit reclosing at the expiration of the fixed dead time or to initiate faster reclosing. If either of the fault detection signals is present or the SAE signal is *not* present at the end of the dead time (2 ms prior to dead-time expiration), the BLOCK_RECLOSE output is asserted. This output can be used to block reclosing and trip all three poles.

Finally, we present simulation results based on EMTP modeling and actual field events. In all simulations, the algorithm either correctly blocks reclosing or identifies SAE within the dead time. These results validate the open-phase voltage analysis and the algorithm's performance.

VII. Appendix A
Open-Phase Voltage Derivation for an Uncompensated Line

Referring to Fig. 1 and applying Kirchhoff's current law for Phase A, with the convention that current coming to Phase A is positive and current leaving Phase A is negative, we get:

$$\begin{aligned}&-V_{AS}\left(0.5Y_{AG}\right)+\left(V_{BS}-V_{AS}\right)\left(0.5Y_{AB}\right)+\\&\left(V_{CS}-V_{AS}\right)\left(0.5Y_{AC}\right)-V_{AR}\left(0.5Y_{AG}\right)+\\&\left(V_{BR}-V_{AR}\right)\left(0.5Y_{AB}\right)+\left(V_{CR}-V_{AR}\right)\left(0.5Y_{AC}\right)=0\end{aligned} \tag{23}$$

The admittances used above have positive imaginary parts, indicating positive values of capacitances. The off-diagonal terms in the Y_{ABC} matrix have negative imaginary parts, so care must be taken to ensure that admittances with positive imaginary values are used in (23). Rearranging (23), we get:

$$V_{AS}+V_{AR}=\frac{\left(V_{BS}+V_{BR}\right)Y_{AB}+\left(V_{CS}+V_{CR}\right)Y_{AC}}{Y_{AB}+Y_{AC}+Y_{AG}} \tag{24}$$

The denominator, representing the sum of the admittances connected to Phase A, ($Y_{AB} + Y_{AC} + Y_{AG}$), is the first term of the Y_{ABC} matrix and can be represented as Y_{AA}. Then (24) can be written as:

$$V_{AS}+V_{AR}=\frac{\left(V_{BS}+V_{BR}\right)Y_{AB}+\left(V_{CS}+V_{CR}\right)Y_{AC}}{Y_{AA}} \tag{25}$$

Equation (25) provides the ES component of the open-phase voltage. The relationship between V_{AS} and V_{AR} can be explored further by applying Kirchhoff's voltage law on Phase A. Thus, we get:

$$V_{AS}-V_{AR}=I'_{AS}Z_{AA}+I'_{BS}Z_{AB}+I'_{CS}Z_{AC}$$

I'_{AS} represents the difference in charging current between the sending and receiving ends. It is relatively small compared to healthy phase load currents and can be ignored. Thus, we can write:

$$V_{AS}-V_{AR}=I'_{BS}Z_{AB}+I'_{CS}Z_{AC} \tag{26}$$

Equation (26) provides the EM component of the open-phase voltage. Here, I'_{BS} and I'_{CS} refer to the current flowing through Phase B and C, respectively, after the charging current is compensated. I'_{BS} can be written as:

$$\begin{aligned}I'_{BS}=I_{BS}-V_{BS}\left(0.5Y_{BG}\right)+\left(V_{AS}-V_{BS}\right)\left(0.5Y_{AB}\right)\\+\left(V_{CS}-V_{BS}\right)\left(0.5Y_{BC}\right)\end{aligned}$$

Rearranging terms, we get:

$$\begin{aligned}I'_{BS}=I_{BS}-\frac{V_{BS}\left(Y_{BG}+Y_{BC}+Y_{AB}\right)}{2}\\+\frac{V_{AS}Y_{AB}}{2}+\frac{V_{CS}Y_{BC}}{2}\end{aligned}$$

In the above expression, $Y_{BG} + Y_{BC} + Y_{AB}$ can be replaced with Y_{BB}, the total admittance connected to Phase B. Furthermore, the voltage V_{AS} is typically small (8 percent to 20 percent of

nominal voltage) and can be ignored for simplicity. Applying these simplifications, we get:

$$I'_{BS} = I_{BS} - \frac{V_{BS}Y_{BB}}{2} + \frac{V_{CS}Y_{BC}}{2} \tag{27}$$

Similarly, we can write the following for I'_{CS}:

$$I'_{CS} = I_{CS} - \frac{V_{CS}Y_{CC}}{2} + \frac{V_{BS}Y_{BC}}{2} \tag{28}$$

Substituting these values in (26), we get:

$$\begin{aligned} V_{AS} - V_{AR} = &\left(I_{BS} - \frac{V_{BS}Y_{BB}}{2} + \frac{V_{CS}Y_{BC}}{2} \right) Z_{AB} \\ &+ \left(I_{CS} - \frac{V_{CS}Y_{CC}}{2} + \frac{V_{BS}Y_{BC}}{2} \right) Z_{AC} \end{aligned} \tag{29}$$

Adding (25) and (29), we get:

$$\begin{aligned} V_{AS} = &\left(I_{BS} - \frac{V_{BS}Y_{BB}}{2} + \frac{V_{CS}Y_{BC}}{2} \right)\left(\frac{Z_{AB}}{2} \right) \\ &+ \left(I_{CS} - \frac{V_{CS}Y_{CC}}{2} + \frac{V_{BS}Y_{BC}}{2} \right)\left(\frac{Z_{AC}}{2} \right) \\ &+ \frac{\left(\frac{V_{BS}+V_{BR}}{2} \right)Y_{AB} + \left(\frac{V_{CS}+V_{CR}}{2} \right)Y_{AC}}{Y_{AA}} \end{aligned} \tag{30}$$

The above expression provides a good match with simulation results for a variety of load conditions, line lengths, etc. If it is desired to only use local quantities (referred to as the sending end here), the remote healthy phase voltages can be derived as follows. For Phase B, we can write the following using Kirchhoff's voltage law (after neglecting the EM component because of the relatively small I'_{AS}):

$$\begin{aligned} &V_{BS} - V_{BR} = I'_{BS}Z_{BB} + I'_{CS}Z_{BC} \\ &\Rightarrow V_{BS} - V_{BR} = \left(I_{BS} - \frac{V_{BS}Y_{BB}}{2} + \frac{V_{CS}Y_{BC}}{2} \right) Z_{BB} \\ &+ \left(I_{CS} - \frac{V_{CS}Y_{CC}}{2} + \frac{V_{BS}Y_{BC}}{2} \right) Z_{BC} \\ &\Rightarrow V_{BR} = V_{BS}\left(1 + \frac{Y_{BB}Z_{BB}}{2} - \frac{Y_{BC}Z_{BC}}{2} \right) \\ &+ V_{CS}\left(\frac{Y_{CC}Z_{BC}}{2} - \frac{Y_{BC}Z_{BB}}{2} \right) \\ &- I_{BS}Z_{BB} - I_{CS}Z_{BC} \end{aligned} \tag{31}$$

Similarly, V_{CR} can be written as:

$$\begin{aligned} V_{CR} = &V_{CS}\left(1 + \frac{Y_{CC}Z_{CC}}{2} - \frac{Y_{BC}Z_{BC}}{2} \right) \\ &+ V_{BS}\left(\frac{Y_{BB}Z_{BC}}{2} - \frac{Y_{BC}Z_{CC}}{2} \right) \\ &- I_{CS}Z_{CC} - I_{BS}Z_{BC} \end{aligned} \tag{32}$$

The values for V_{BR} and V_{CR} from (31) and (32) can be used in (30) to calculate the open-phase voltage by using only locally measured quantities.

Equation (30) provides the accurate expression for an untransposed line. Next, we try to simplify (30) with some simplifying assumptions. If a line is short, such that its charging current is very small compared to the load, then (30) can be simplified by removing the charging-current compensation from I_{BS} and I_{CS}, as shown in (33).

$$\begin{aligned} V_{AS} = &\left(\frac{I_{BS}Z_{AB} + I_{CS}Z_{AC}}{2} \right) \\ &+ \frac{\left(\frac{V_{BS}+V_{BR}}{2} \right)Y_{AB} + \left(\frac{V_{CS}+V_{CR}}{2} \right)Y_{AC}}{Y_{AA}} \end{aligned} \tag{33}$$

The first part of (33) provides the contribution of EM coupling to the open-phase voltage due to currents in the other two phases, and the second part provides the contribution of ES coupling from the healthy phases. Simplifying the equation further, we can write $Y_{[pp]}$ as $2\pi fC[pp]$:

$$\begin{aligned} V_{AS} = &\left(\frac{I_{BS}Z_{AB} + I_{CS}Z_{AC}}{2} \right) \\ &+ \frac{\left(\frac{V_{BS}+V_{BR}}{2} \right)C_{AB} + \left(\frac{V_{CS}+V_{CR}}{2} \right)C_{AC}}{C_{AA}} \end{aligned} \tag{34}$$

If the line is transposed, then:

$$\begin{aligned} Z_{AB} = Z_{AC} = Z_M &= (Z_0 - Z_1)/3 \\ C_{AB} = C_{AC} = C_M &= (C_1 - C_0)/3 \\ C_{AA} = C_S &= (2C_1 + C_0)/3 \end{aligned} \tag{35}$$

Also, let $(V_{BS} + V_{BR}) / 2 = V_{B_{avg}}$ and $(V_{CS} + V_{CR}) / 2 = V_{C_{avg}}$, representing average voltages. Substituting these and (35) into (34), we get the following for a transposed line:

$$\begin{aligned} V_{AS} = &\left(\frac{I_{BS} + I_{CS}}{2} \right)\left(\frac{Z_0 - Z_1}{3} \right) \\ &+ \left(V_{B_{avg}} + V_{C_{avg}} \right)\left(\frac{C_1 - C_0}{2C_1 + C_0} \right) \end{aligned} \tag{36}$$

VIII. Appendix B
Open-Phase Voltage Derivation for a Compensated Line

In this section, we analyze the open-phase voltage in a transposed shunt-reactor-compensated line. We assume the shunt reactor bank to be a four-legged reactor bank available on both ends of the line with the same sizing. Consider the circuit diagram shown in Fig. 2.

Applying Kirchhoff's current law for Phase A, we get:

$$-V_{AS}\left(\frac{Y_G}{2}\right)+\left(V_{BS}-V_{AS}\right)\left(\frac{Y_M}{2}\right)$$
$$+\left(V_{CS}-V_{AS}\right)\left(\frac{Y_M}{2}\right)-\frac{V_{AS}-V_{NS}}{2Z_P}+$$
$$-V_{AR}\left(\frac{Y_G}{2}\right)+\left(V_{BR}-V_{AR}\right)\left(\frac{Y_M}{2}\right)$$
$$+\left(V_{CR}-V_{AR}\right)\left(\frac{Y_M}{2}\right)-\frac{V_{AR}-V_{NR}}{2Z_P}=0$$

Rearranging terms, we get:

$$\left(V_{AS}+V_{AR}\right)\left(Y_G+2Y_M+\frac{1}{Z_P}\right)$$
$$=\left(V_{BS}+V_{BR}\right)Y_M+\left(V_{CS}+V_{CR}\right)Y_M+\frac{V_{NS}+V_{NR}}{Z_P}$$

The term $Y_G + 2Y_M$ refers to the self-admittance, Y_S. Substituting this, we get:

$$\left(V_{AS}+V_{AR}\right)\left(Y_S+\frac{1}{Z_P}\right)$$
$$=\left(V_{BS}+V_{BR}\right)Y_M+\left(V_{CS}+V_{CR}\right)Y_M+\frac{V_{NS}+V_{NR}}{Z_P} \quad (37)$$

where Z_P refers to the impedance of the phase reactor and V_{NS} is the voltage across the sending end neutral reactor. The reactor voltage can be written as:

$$V_{NS}=\left(\frac{V_{AS}-V_{NS}}{2Z_P}+\frac{V_{BS}-V_{NS}}{2Z_P}+\frac{V_{CS}-V_{NS}}{2Z_P}\right)\left(2Z_N\right)$$

where Z_N is the neutral reactor impedance. The equation can then be rearranged as shown in (38).

$$V_{NS}\left(1+\frac{3Z_N}{Z_P}\right)=\frac{\left(V_{AS}+V_{BS}+V_{CS}\right)Z_N}{Z_P}$$
$$V_{NS}=\frac{\left(V_{AS}+V_{BS}+V_{CS}\right)Z_N}{Z_P+3Z_N} \quad (38)$$

Similarly, we can write the following for V_{NR}:

$$V_{NR}=\frac{\left(V_{AR}+V_{BR}+V_{CR}\right)Z_N}{Z_P+3Z_N} \quad (39)$$

Substituting the expressions for V_{NS} and V_{NR} in (37), we get:

$$\left(V_{AS}+V_{AR}\right)\left(Y_S+\frac{1}{Z_P}\right)=\left(V_{BS}+V_{BR}\right)Y_M$$
$$+\left(V_{CS}+V_{CR}\right)Y_M$$
$$+\frac{\left(\frac{\left(V_{AS}+V_{BS}+V_{CS}\right)Z_N}{Z_P+3Z_N}+\frac{\left(V_{AR}+V_{BR}+V_{CR}\right)Z_N}{Z_P+3Z_N}\right)}{Z_P}$$

Rearranging, we get:

$$\left(V_{AS}+V_{AR}\right)\left(Y_S+\frac{1}{Z_P}-\frac{Z_N}{Z_P\left(Z_P+3Z_N\right)}\right)$$
$$=\left(V_{BS}+V_{BR}\right)\left(Y_M+\frac{Z_N}{Z_P\left(Z_P+3Z_N\right)}\right)$$
$$+\left(V_{CS}+V_{CR}\right)\left(Y_M+\frac{Z_N}{Z_P\left(Z_P+3Z_N\right)}\right)$$

Simplifying further, we get:

$$\left(V_{AS}+V_{AR}\right)\left(Y_S+\frac{Z_P+2Z_N}{Z_P\left(Z_P+3Z_N\right)}\right)$$
$$=\left(V_{BS}+V_{BR}\right)\left(Y_M+\frac{Z_N}{Z_P\left(Z_P+3Z_N\right)}\right) \quad (40)$$
$$+\left(V_{CS}+V_{CR}\right)\left(Y_M+\frac{Z_N}{Z_P\left(Z_P+3Z_N\right)}\right)$$

Let us define a few constants to simplify the expressions:

$$Y_S'=Y_S+\frac{Z_P+2Z_N}{Z_P\left(Z_P+3Z_N\right)}$$
$$Y_M'=Y_M+\frac{Z_N}{Z_P\left(Z_P+3Z_N\right)} \quad (41)$$

Substituting (41) in (40), we get:

$$V_{AS}+V_{AR}=\frac{\left(V_{BS}+V_{BR}\right)Y_M'+\left(V_{CS}+V_{CR}\right)Y_M'}{Y_S'} \quad (42)$$

Equation (42) is very similar in form to (25). Equation (42) provides the contribution of ES coupling to the open-phase voltage. It can be seen from (41) that the presence of a neutral reactor (Z_N) tends to cancel the effect of the mutual capacitance because we are adding capacitive and inductive admittances, which tend to cancel and reduce the original admittance. The size of the neutral reactor that completely cancels the mutual capacitance can be determined by forcing Y'_M in (41) to 0, as shown in (43):

$$Y_M+\frac{Z_N}{Z_P\left(Z_P+3Z_N\right)}=0 \quad (43)$$

Ignoring the resistance and recognizing that the capacitive and inductive terms have opposing signs, it suffices to equate the magnitudes as follows:

$$\left|\frac{Z_N}{Z_P\left(Z_P+3Z_N\right)}\right|=\left|Y_M\right|$$

Converting these to their respective capacitances and inductances using $\omega = 2\pi f$, we get:

$$\left|\frac{\omega L_N}{\left(\omega L_P\right)\left(\omega L_P+3\omega L_N\right)}\right|=\left|\omega C_M\right|$$

Simplifying the above, we get:

$$\frac{L_N}{L_P\left(L_P+3L_N\right)}=\omega^2C_M$$
$$\Rightarrow L_N=\omega^2C_M\left(L_P\left(L_P+3L_N\right)\right)$$
$$\Rightarrow L_N\left(1-3\omega^2L_PC_M\right)=\omega^2C_ML_P^2$$

Thus we get for L_N:

$$L_N=\frac{\omega^2C_ML_P^2}{1-3\omega^2L_PC_M} \tag{44}$$

We can explore (43) more to get a different expression for Z_N that is more commonly seen in other papers [2] [12]. To do so, let us rewrite (43) as:

$$Z_N=\frac{Z_P^2Y_M}{1-3Z_PY_M} \tag{45}$$

Then, let us replace Y_M with $\frac{B_1-B_0}{3}$ and let $\frac{1}{Z_P}$ be some "$Comp_{pu}$" fraction of capacitive susceptance, i.e.:

$$\frac{1}{Z_P}=Comp_{pu}B_1\Rightarrow Z_P=\frac{1}{Comp_{pu}B_1} \tag{46}$$

Finally, substituting the above in (45), we get:

$$Z_N=\frac{\left(B_1-B_0\right)}{3Comp_{pu}^2B_1^2\left(1-\frac{3\left(B_1-B_0\right)}{3Comp_{pu}B_1}\right)}$$
$$\Rightarrow Z_N=\frac{\left(B_1-B_0\right)}{3Comp_{pu}B_1\left(Comp_{pu}B_1-B_1+B_0\right)}$$
$$\Rightarrow Z_N=\frac{B_1-B_0}{3Comp_{pu}B_1\left(B_0-\left(1-Comp_{pu}\right)B_1\right)}$$

The EM part of the open-phase voltage is affected as well because of the introduction of shunt reactors. We need to account for both the capacitive charging current and the inductive reactor current in order to accurately estimate the portion of the measured current that contributes to the EM coupling. Recall from (26) that currents used in mutual coupling voltage terms were charging-current compensated. Thus, referring to Fig. 2 and using (27), we get the following for I'_{BS}:

$$I'_{BS}=I_{BS}-\frac{V_{BS}Y_S}{2}+\frac{V_{CS}Y_M}{2}-\frac{V_{BS}V_{NS}}{2Z_P}$$

Substituting the value of V_{NS} from (38), we get:

$$I'_{BS}=I_{BS}-\frac{V_{BS}Y_S}{2}+\frac{V_{CS}Y_M}{2}-\frac{V_{BS}-\left(\frac{\left(V_{AS}+V_{BS}+V_{CS}\right)Z_N}{Z_P+3Z_N}\right)}{2Z_P}$$

We can substitute V_{AS} with 0 because the effect of the low open-Phase-A voltage is small. Then we get:

$$I'_{BS}=I_{BS}-\frac{V_{BS}Y_S}{2}+\frac{V_{CS}Y_M}{2}-\frac{V_{BS}-\left(\frac{\left(V_{BS}+V_{CS}\right)Z_N}{Z_P+3Z_N}\right)}{2Z_P}$$

Rearranging, we get:

$$I'_{BS}=I_{BS}-V_{BS}\left(\frac{Y_S}{2}+\frac{Z_P+2Z_N}{2Z_P\left(Z_P+3Z_N\right)}\right)+V_{CS}\left(\frac{Y_M}{2}+\frac{Z_N}{2Z_P\left(Z_P+3Z_N\right)}\right)$$

Similarly, for I'_{CS}, we get:

$$I'_{CS}=I_{CS}-V_{CS}\left(\frac{Y_S}{2}+\frac{Z_P+2Z_N}{2Z_P\left(Z_P+3Z_N\right)}\right)+V_{BS}\left(\frac{Y_M}{2}+\frac{Z_N}{2Z_P\left(Z_P+3Z_N\right)}\right)$$

Substituting the values of I'_{BS} and I'_{CS} into (26), we get:

$$V_{AS}-V_{AR}=\left[\begin{array}{l}I_{BS}-V_{BS}\left(\frac{Y_S}{2}+\frac{Z_P+2Z_N}{2Z_P\left(Z_P+3Z_N\right)}\right)\\+V_{CS}\left(\frac{Y_M}{2}+\frac{Z_N}{2Z_P\left(Z_P+3Z_N\right)}\right)\end{array}\right]Z_M+\left[\begin{array}{l}I_{CS}-V_{CS}\left(\frac{Y_S}{2}+\frac{Z_P+2Z_N}{2Z_P\left(Z_P+3Z_N\right)}\right)\\+V_{BS}\left(\frac{Y_M}{2}+\frac{Z_N}{2Z_P\left(Z_P+3Z_N\right)}\right)\end{array}\right]Z_M \tag{47}$$

Using the definitions of (41), we can rewrite (47) as:

$$V_{AS}-V_{AR}=\left(I_{BS}-\frac{V_{BS}Y'_S}{2}+\frac{V_{CS}Y'_M}{2}\right)Z_M+\left(I_{CS}-\frac{V_{CS}Y'_S}{2}+\frac{V_{BS}Y'_M}{2}\right)Z_M \tag{48}$$

Equation (48) is very similar in form to (29). Combining (42) and (48), we can write the following for V_{AS}:

$$V_{AS}=\left(I_{BS}-\frac{V_{BS}Y'_S}{2}+\frac{V_{CS}Y'_M}{2}\right)\left(\frac{Z_M}{2}\right)+\left(I_{CS}-\frac{V_{CS}Y'_S}{2}+\frac{V_{BS}Y'_M}{2}\right)\left(\frac{Z_M}{2}\right)+\frac{\left(\frac{V_{BS}+V_{BR}}{2}\right)Y'_M+\left(\frac{V_{CS}+V_{CR}}{2}\right)Y'_M}{Y'_S} \tag{49}$$

IX. Appendix C
Open-Phase Voltage in Uncompensated Lines During Faults

Consider a fault with fault resistance R_f that exists at location m (per-unit line length) from the sending end of an uncompensated untransposed transmission line, as shown in Fig. 3. The open-phase voltage can be derived using Kirchhoff's voltage law as follows:

$$\begin{aligned} V_{AS} &= mZ_{AA}I_{AS} + mZ_{AB}I'_{BS} + mZ_{AC}I'_{CS} \\ &\quad + R_f\left(I_{AS} + I_{AR}\right) \\ V_{AS} &= I_{AS}\left(mZ_{AA} + R_f\right) + mZ_{AB}I'_{BS} + mZ_{AC}I'_{CS} \\ &\quad + R_f I_{AR} \end{aligned} \tag{50}$$

I_{AS} can be derived as:

$$\begin{aligned} I_{AS} &= -mY_{AG}V_{AS} + mY_{AB}\left(V_{BS} - V_{AS}\right) \\ &\quad + mY_{AC}\left(V_{CS} - V_{AS}\right) \\ &\Rightarrow I_{AS} = -m\left(Y_{AG} + Y_{AB} + Y_{AC}\right)V_{AS} + mY_{AB}V_{BS} \\ &\quad + mY_{AC}V_{CS} \end{aligned}$$

$Y_{AG} + Y_{AB} + Y_{AC}$ can be written as Y_{AA}, and the above can be simplified as:

$$\begin{aligned} I_{AS} &= -mY_{AA}V_{AS} + mY_{AB}V_{BS} + mY_{AC}V_{CS} \\ I_{AS} &= m\left(-Y_{AA}V_{AS} + Y_{AB}V_{BS} + Y_{AC}V_{CS}\right) \end{aligned} \tag{51}$$

Substituting the value of I_{AS} into (50), we get:

$$\begin{aligned} V_{AS} &= m\left(-Y_{AA}V_{AS} + Y_{AB}V_{BS} + Y_{AC}V_{CS}\right)\left(mZ_{AA} + R_f\right) \\ &\quad + mZ_{AB}I'_{BS} + mZ_{AC}I'_{CS} + R_f I_{AR} \\ &\Rightarrow V_{AS}\left(1 + mY_{AA}\left(mZ_{AA} + R_f\right)\right) \\ &= m\left(Y_{AB}V_{BS} + Y_{AC}V_{CS}\right)\left(mZ_{AA} + R_f\right) \\ &\quad + mZ_{AB}I'_{BS} + mZ_{AC}I'_{CS} + R_f I_{AR} \\ V_{AS} &= \frac{m\left(Y_{AB}V_{BS} + Y_{AC}V_{CS}\right)\left(mZ_{AA} + R_f\right)}{1 + mY_{AA}\left(mZ_{AA} + R_f\right)} \\ &\quad + \frac{m\left(Z_{AB}I'_{BS} + Z_{AC}I'_{CS}\right)}{1 + mY_{AA}\left(mZ_{AA} + R_f\right)} \\ &\quad + \frac{R_f I_{AR}}{1 + mY_{AA}\left(mZ_{AA} + R_f\right)} \end{aligned} \tag{52}$$

X. Appendix D
Ringing Circuit Analysis

The aim of this analysis is to reduce the circuit so that ringing can be analyzed. We start with a simplified circuit diagram of a transposed transmission line compensated with a four-reactor bank on both ends of the line, as shown in Fig. 40. The quantities used in the circuit are already defined in Subsection II.D. For simplicity, we ignore the line impedance because line impedance values are typically much smaller than shunt reactor values.

We can then fold this circuit around the fault point so that all the capacitances and inductances on either side of the fault come in parallel with their mirrored counterparts. Further, because ringing does not include any forced component, we can short all the voltage sources to ground. Thus, we reduce the circuit in Fig. 40 to that shown in Fig. 41. We can further reduce Fig. 41 to a very simple parallel RLC circuit as shown in Fig. 42, after realizing that at point N, L_N comes in parallel with two L_Ps connected between point N and ground.

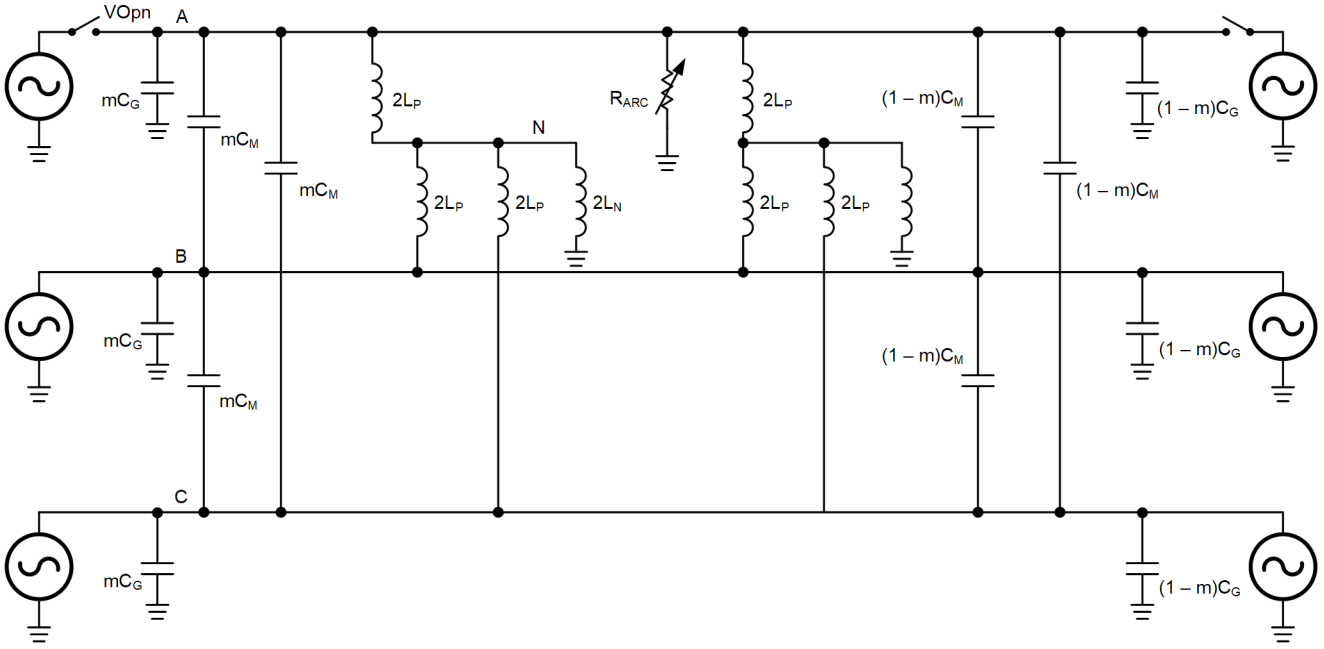

Fig. 40. Simplified Circuit Representation of a Compensated Transmission Line

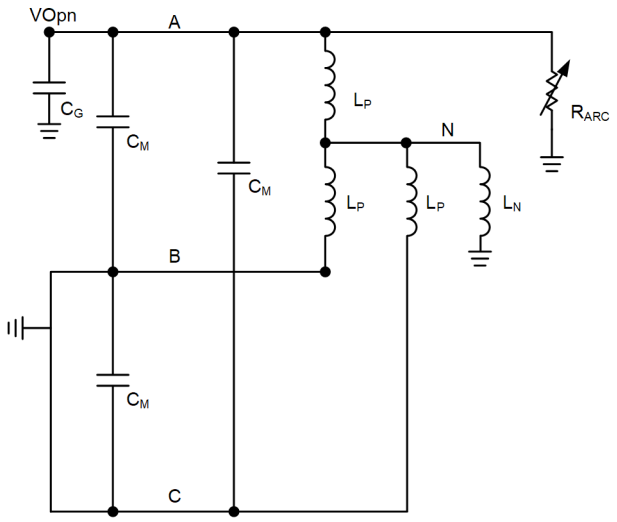

Fig. 41. Reduced Circuit Representation of a Compensated Transmission Line

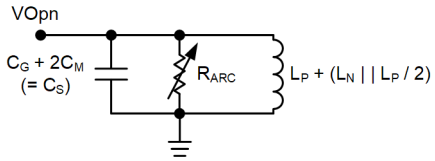

Fig. 42. Equivalent Circuit Representation of a Compensated Transmission Line

The ringing occurs as a result of oscillation between the equivalent inductance and capacitance once the arc is extinguished (i.e., when R_{ARC} is removed from the circuit in Fig. 42). The frequency of this oscillation can be determined as shown in (53).

$$F_{RING} = \frac{1}{2\pi\sqrt{(C_S)\left[\frac{L_P(L_P+3L_N)}{L_P+2L_N}\right]}} \tag{53}$$

Equation (53) can be simplified further. Let us first consider the right side quantity with L_P and L_N. Substituting the value of L_N from (44), we get:

$$\frac{L_P+3L_N}{L_P+2L_N} = \frac{L_P+3\left[\frac{\omega^2 C_M L_P^2}{1-3\omega^2 L_P C_M}\right]}{L_P+2\left[\frac{\omega^2 C_M L_P^2}{1-3\omega^2 L_P C_M}\right]} = \frac{L_P}{L_P-\omega^2 L_P^2 C_M} \tag{54}$$

$$\Rightarrow \frac{L_P+3L_N}{L_P+2L_N} = \frac{1}{1-\omega^2 L_P C_M}$$

Recall from (46) the following:

$$\frac{1}{Z_P} = \text{Comp}_{pu} B_1$$

This can be written in terms of inductances and capacitances, as shown in (55):

$$\frac{1}{\omega L_P} = \text{Comp}_{pu}\,\omega C_1 \Rightarrow \omega^2 L_P = \frac{1}{\text{Comp}_{pu} C_1} \tag{55}$$

Substituting the above in (54), we get:

$$\frac{L_P+3L_N}{L_P+2L_N} = \frac{1}{1-\omega^2 L_P C_M} = \frac{1}{1-\frac{C_M}{\text{Comp}_{pu} C_1}}$$

Substituting the above in (53), we get:

$$F_{RING} = \frac{1}{2\pi\sqrt{(C_S)\left[\frac{L_P(L_P+3L_N)}{L_P+2L_N}\right]}} = \frac{1}{2\pi\sqrt{\frac{C_S L_P}{\left(1-\frac{C_M}{\text{Comp}_{pu} C_1}\right)}}}$$

For higher levels of shunt-reactor compensation, Comp_{pu} can be approximated as 1, then we get:

$$F_{RING} \approx \frac{1}{2\pi\sqrt{\frac{C_S L_P}{\left(1-\frac{C_M}{C_1}\right)}}} = \frac{1}{2\pi\sqrt{\frac{C_S L_P C_1}{C_1-C_M}}} = \frac{1}{2\pi\sqrt{\frac{C_S L_P C_1}{C_S}}}$$

The last part follows from the fact that $C_1 = C_S - C_M$. Thus, we finally have a simpler expression for F_{RING}, as shown in (56).

$$F_{RING} \approx \frac{1}{2\pi\sqrt{L_P C_1}} \tag{56}$$

Substituting L_P from (55), we get:

$$F_{RING} \approx \frac{1}{2\pi\sqrt{\frac{C_1}{\omega^2 \text{Comp}_{pu} C_1}}} = \frac{\omega}{2\pi}\sqrt{\text{Comp}_{pu}} = F_{NOM}\sqrt{\text{Comp}_{pu}} \tag{57}$$

Fig. 43 provides a comparison of ringing frequency by comparing (53) (accurate equation) and (56) (approximate equation) against the actual frequency, as observed from simulations.

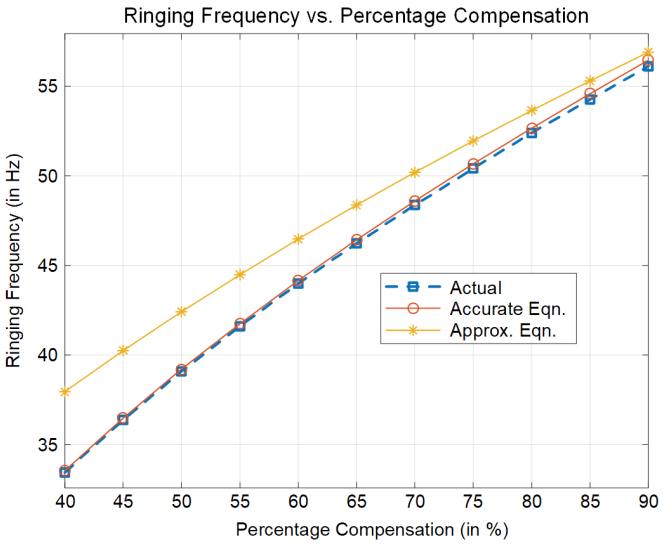

Fig. 43. Comparison of Ringing Frequencies to Actual Simulation Values

XI. Appendix E
Derivation of a Leakage Factor for the Modified Harmonic Distortion Calculator

The modification in the Harm_Dist calculation can be understood as follows: Assuming that the actual rms sum of harmonics in the open-phase voltage signal is V_{HARM} and that the fundamental frequency steady-state open-phase voltage magnitude is V_{MEAN}, the comparison to evaluate HARM_DIST_HI is shown in (58).

$$HARM\_DIST\_HI = V_{HARM} > 0.05 \bullet V_{MEAN} \tag{58}$$

However, the measured harmonic content ($V_{HARM_{Meas}}$) will contain the leakage from the ringing component of the open-phase voltage. This component is approximately a leakage factor (LkgFact) times the magnitude of the estimated ringing component magnitude, V_{RING}. The leakage factor is estimated from the gain of the frequency responses of the harmonic filters at the ringing frequency, F_{RING}. This is shown in (59). The LkgFact at oscillation frequency, F_{RING}, is given by (60), where H[n](F) denotes the frequency response for nth harmonic filter evaluated at frequency F.

$$V_{HARM_{Meas}} \approx V_{HARM} + LkgFact \bullet V_{RING} \tag{59}$$

$$LkgFact = \frac{}{\sqrt{\left|H2(F_{RING})\right|^2 + \left|H3(F_{RING})\right|^2 + \left|H4(F_{RING})\right|^2 + \left|H5(F_{RING})\right|^2}} \tag{60}$$

The second part of (59) thus provides the adaptive component to be used in order to get the desired comparison of (58). To see this, consider the following comparison with an adaptive threshold:

$$V_{HARM_{Meas}} > 0.05 \bullet V_{MEAN} + Adaptive\_Component$$

Substituting the expression for $V_{HARM_{Meas}}$ from (59), we get:

$$\begin{aligned} &V_{HARM} + LkgFact \bullet V_{RING} > \\ &0.05 \bullet V_{MEAN} + Adaptive\_Component \end{aligned} \tag{61}$$

Let us choose the Adaptive Component as shown below and substitute it in the equation above:

$$Adaptive\_Component = LkgFact \bullet V_{RING} \tag{62}$$

Substituting (62) in (61), we get:

$$\begin{aligned} &V_{HARM} + LkgFact \bullet V_{RING} > \\ &0.05 \bullet V_{MEAN} + LkgFact \bullet V_{RING} \\ &\Rightarrow HARM\_DIST\_HI = V_{HARM} > 0.05 \bullet V_{MEAN} \end{aligned}$$

which is same as the desired comparison in (58).

XII. Appendix F
Tables of Comprehensive Test Cases, Tower Configuration, and Line Parameters

Table I
Comprehensive Test Case Parameters and Their Ranges

Parameter Name	Line Configuration			
	Uncompensated, Untransposed	**Uncompensated, Transposed**	**Compensated, Transposed**	**Compensated, Untransposed**
Voltage Level (kV)	[132, 220, 400, 765]	[132, 220, 400, 765]	[132, 220, 400, 765]	[132, 220, 400, 765]
Line Length (km)	[30, 300]	[30, 300]	[300, 500]	[300, 500]
Fault Location (pu)	[0.1, 0.5, 0.9]	[0.1, 0.5, 0.9]	[0.1, 0.5, 0.9]	[0.1, 0.5, 0.9]
Phase	[A, B, C]	A	A	[A, B, C]
Loading (Remote Bus Angle (degrees))	[–30, –10, 0, 10, 30]	[–30, –10, 0, 10, 30]	[–30, –10, 0, 10, 30]	[–30, –10, 0, 10, 30]
Source Impedance Ratio (Mag)	[0.1, 1, 10]	[0.1, 1, 10]	[0.1, 1, 10]	[0.1, 1, 10]
Percentage Compensation	Not Applicable	Not Applicable	[50, 75, 90]	[50, 75, 90]
Reactors in Service	Not Applicable	Not Applicable	[Local, Remote, Both]	[Local, Remote, Both]

Table II
Tower Configuration (132 kV Line)

Cond #	132 kV Tower Configuration Data (as entered in ATPDraw)									
	Ph. no.	**Rin (in)**	**Rout (in)**	**Resistivity (Ω/mi DC)**	**Horizontal (ft)**	**Vtower (ft)**	**Vmid (ft)**	**Separation (in)**	**Alpha (deg)**	**NB**
1	1	0	0.588	0.1083	25.59	42.65	28.43	0	0	1
2	2	0	0.588	0.1083	0	49.21	32.81	0	0	1
3	3	0	0.588	0.1083	22.31	55.77	37.18	0	0	1

TABLE III
TOWER CONFIGURATION (220 KV LINE)

Cond #	220 kV Tower Configuration Data (as entered in ATPDraw)									
	Ph. no.	**Rin (in)**	**Rout (in)**	**Resistivity (Ω/mi DC)**	**Horizontal (ft)**	**Vtower (ft)**	**Vmid (ft)**	**Separation (in)**	**Alpha (deg)**	**NB**
1	1	0	0.563	0.1085	0	64.4	35.14	11.42	0	2
2	2	0	0.563	0.1085	41.4	64.4	35.14	11.42	0	2
3	3	0	0.563	0.1085	1.15	83.10	53.84	11.42	0	2
4	0	0	0.162	1.372	20.67	123.46	108.37	0	0	1

TABLE IV
TOWER CONFIGURATION (400 KV LINE)

Cond #	400 kV Tower Configuration Data (as entered in ATPDraw)									
	Ph. no.	**Rin (in)**	**Rout (in)**	**Resistivity (Ω/mi DC)**	**Horizontal (ft)**	**Vtower (ft)**	**Vmid (ft)**	**Separation (in)**	**Alpha (deg)**	**NB**
1	1	0	0.625	0.088	0	71.52	29	12.60	45	4
2	2	0	0.625	0.088	36.09	71.52	29	12.60	45	4
3	3	0	0.625	0.088	72.18	71.52	29	12.60	45	4
4	0	0	0.162	1.372	9.74	96.03	56.66	0	0	1
5	0	0	0.162	1.372	62.43	96.03	56.66	0	0	1

TABLE V
TOWER CONFIGURATION (765 KV LINE)

Cond #	765 kV Tower Configuration Data (as entered in ATPDraw)									
	Ph. no.	**Rin (in)**	**Rout (in)**	**Resistivity (Ω/mi DC)**	**Horizontal (ft)**	**Vtower (ft)**	**Vmid (ft)**	**Separation (in)**	**Alpha (deg)**	**NB**
1	1	0	0.503	0.016	0	115	50	15	30	6
2	2	0	0.503	0.016	45	115	50	15	30	6
3	0	0	0.503	0.016	90	115	50	15	30	6
4	0	0	0.323	0.646	0	155	105	0	0	1
5	0	0	0.323	0.646	90	155	105	0	0	1

TABLE VI
LINE PARAMETERS

Parameter	Voltage Level (kV)			
	132	220	400	765
ZAA (ohms/mi)	1.37∠81.49°	1.09∠80.30°	0.86∠77.96°	0.77∠82.43°
ZAB (ohms/mi)	0.58∠80.75°	0.44∠73.07°	0.36∠63.89°	0.31∠71.89°
ZCA (ohms/mi)	0.68∠82.22°	0.53∠75.53°	0.29∠58.49°	0.24∠66.62°
ZBB (ohms/mi)	1.38∠81.50°	1.09∠80.30°	0.85∠77.48°	0.77∠82.40°
ZBC (ohms/mi)	0.59∠81.04°	0.43∠72.04°	0.36∠63.89°	0.31∠71.89°
ZCC (ohms/mi)	1.38∠81.52°	1.08∠79.79°	0.86∠77.96°	0.77∠82.43°
ZS (ohms/mi)	1.38∠81.50°	1.09∠80.13°	0.86∠77.80°	0.77∠82.42°
ZM (ohms/mi)	0.62∠81.39°	0.46∠73.68°	0.34∠62.34°	0.29∠70.44°
YAA (µmho/mi)	5.10∠90°	6.15∠90°	7.15∠90°	7.41∠90°
YAB (µmho/mi)	0.52∠90°	0.61∠90°	1.04∠90°	1.44∠90°
YCA (µmho/mi)	1.25∠90°	1.55∠90°	0.25∠90°	0.39∠90°
YBB (µmho/mi)	4.79∠90°	5.81∠90°	7.31∠90°	7.66∠90°
YBC (µmho/mi)	0.70∠90°	0.64∠90°	1.04∠90°	1.44∠90°
YCC (µmho/mi)	4.96∠90°	5.90∠90°	7.15∠90°	7.41∠90°
YS (µmho/mi)	4.95∠90°	5.95∠90°	7.20∠90°	7.49∠90°
YM (µmho/mi)	0.82∠90°	0.93∠90°	0.78∠90°	1.09∠90°

XIII. ACKNOWLEDGMENT

We thank Normann Fischer, Armando Guzmán, Daqing Hou, Bernard Matta, Kamal Garg, Austin Wade, and Adam Sylvia for their careful review and helpful comments. We also thank CFE for sharing field events and transmission line data.

XIV. REFERENCES

[1] IEEE Power System Relaying Committee Working Group, "Single Phase Tripping and Auto Reclosing of Transmission Lines—IEEE Committee Report," *IEEE Transactions on Power Delivery*, Vol. 7, Issue 1, January 1992, pp. 182–192.

[2] E. W. Kimbark, "Suppression of Ground-Fault Arcs on Single-Pole-Switched EHV Lines by Shunt Reactors," *IEEE Transactions on Power Apparatus and Systems*, Vol. 83, Issue 3, March 1964, pp. 285–290.

[3] N. Knudsen, "Single Phase Switching of Transmission Lines Using Reactors for Extinction of the Secondary Arc," CIGRE, no. 310, 1962.

[4] A. M. Al-Rawi, "Simulation of Secondary Arcs in EHV Systems Employing Single-Pole Autoreclosure," Ph.D. dissertation, Dept. of Electronic and Electrical Engineering, University of Bath, UK, 1981.

[5] E. A. Fakheri, B. J. Ware, and B. R. Shperling, "Compensation Scheme for Single-Pole Switching on Untransposed Transmission Lines," *IEEE Transactions on Power Apparatus and Systems*, Vol. PAS-97, Issue 4, July 1978, pp. 1421–1429.

[6] B. R. Shperling and A. Fakheri, "Single-Phase Switching Parameters for Untransposed EHV Transmission Lines," *IEEE Transactions on Power Apparatus and Systems*, Vol. PAS-98, Issue 2, March 1979, pp. 643–654.

[7] R. M. Hasibar, A. C. Legate, J. Brunke, and W. G. Peterson, "The Application of High-Speed Grounding Switches for Single-Pole Reclosing on 500 kV Power Systems," *IEEE Transactions on Power Apparatus and Systems*, Vol. PAS-100, Issue 4, April 1981, pp. 1512–1515.

[8] D. S. Maragal, "Universal Adaptive Automatic Reclosure Techniques for Transmission Lines," Ph.D. dissertation, Polytechnic Institute of New York University, NY, 2013.

[9] A. A. Montanari, M. C. Tavares, and C. M. Portela, "Adaptative Single-Phase Autoreclosing Based on Secondary Arc Voltage Harmonic Signature," proceedings of the International Conference on Power Systems Transients (IPST), Kyoto, Japan, 2009. Available: https://www.ipstconf.org/papers/Proc_IPST2009/09IPST047.pdf

[10] A. Stinskiy, "Novel Approach to Detect Secondary Arc on Single Pole Tripping Events," proceedings of the 75th Annual Conference for Protective Relay Engineers, College Station, TX, 2022.

[11] E. Godoy, A. Celaya, H. J. Altuve, N. Fischer, and A. Guzmán, "Tutorial on Single-Pole Tripping and Reclosing," proceedings of the 39th Annual Western Protective Relay Conference, Spokane, WA, October 2012.

[12] M. R. D. Zadeh, I. Voloh, M. Kanabar, and Y. Xue, "An Adaptive HV Transmission Lines Reclosing Based on Voltage Pattern in the Complex Plane," proceedings of the 65th Annual Conference for Protective Relay Engineers, College Station, TX, 2012.

[13] M. I. Khoroshev and V. Faybisovich, "Multifactor Adaptive Auto-Reclosing of High Voltage Transmission Lines," U.S. Patent 7 317 599, Jan. 8, 2008.

[14] B. R. Shperling, A. J. Fakheri, C. H. Shih, and B. J. Ware, "Analysis of Single Phase Switching Field Tests on the AEP 765 kV System," *IEEE Transactions on Power Apparatus and Systems*, Vol. PAS-100, Issue 4, April 1981, pp. 1729–1735.

[15] A. T. Johns and W. M. Ritchie, "Application of an Improved Technique for Assessing the Performance of Single-Pole Reclosing Schemes," *IEEE transactions on Power Apparatus and Systems*, Vol. PAS-103, Issue 12, December 1984, pp. 3651–3662.

[16] IEEE Std C37.04-2018, *IEEE Standard for Ratings and Requirements for AC High-Voltage Circuit Breakers With Rated Maximum Voltage Above 1000 V*.

[17] J. Sousa, D. Santos, and M. T. Correia de Barros, "Fault Arc Modeling in EMTP," proceedings of the International Conference on Power Systems Transients (IPST), Lisbon, Portugal, 1995. Available: https://www.ipstconf.org/papers/Proc_IPST1995/95IPST012-27.pdf

[18] S. Goldberg, W. F. Horton, and D. Tziouvaras, "A Computer Model of the Secondary Arc in Single Phase Operation of Transmission Lines," *IEEE Transactions on Power Delivery*, Vol. 4, Issue 1, January 1989, pp. 286–295.

XV. Biographies

Tomas Enrique Velasco Ramirez received his BS in electrical-electronic engineering and MS in electrical power systems from the National Autonomous University of Mexico (known in Mexico as UNAM). Prior to 2011, he worked as an electrical installation design engineer. In 2011 he joined Comisión Federal de Electricidad (CFE) as head of the protection and measurement office and later, in 2016, he served as head of the Grid Analysis department of the central transmission region of CFE. He currently works as head of the Protection department in the Transmission Directorate of CFE. His areas of interest are related to electrical protection, traveling waves, wide-area monitoring systems (WAMS) and wide-area monitoring protection and control systems (WAMPACS), synchrophasors, and analysis and simulation of electric power systems.

Carlos Alberto Vizcaino Nuñez received his BS in mechanical and electrical engineering from the University of Colima, Manzanillo, Mexico, in 2002, and an MS in electrical engineering from the Center for Research and Advanced Studies (CINVESTAV) of the National Polytechnic Institute, Guadalajara, Mexico, in 2004. From 2005 to 2010, he was a field application and commissioning engineer for Comisión Federal de Electricidad (CFE). He is presently the manager of the Protection department in the western region for CFE. His research interests include power system protection and electromagnetic transients modeling and simulation.

Sajal Kumar Harmukh received his BTech degree in electrical power engineering in 2012 from the Indian Institute of Technology Delhi in India and his MS in electrical engineering in 2016 from the University of Illinois at Urbana-Champaign. Previously, he worked for NTPC Limited, India, as an assistant manager in the Operations and Maintenance department. He currently works as a power engineer at Schweitzer Engineering Laboratories, Inc. (SEL).

David Schmidt received his BS in physics from Vanderbilt University in 2000 and his ME in electrical engineering from the University of Idaho in 2017. He joined Schweitzer Engineering Laboratories, Inc. (SEL) in 2009 as a protection engineer and project manager in the SEL Engineering Services, Inc. (SEL ES) group, working on protection and control design and relay settings. He is presently a development engineer in Research and Development working on product development. He is a registered professional engineer in the states of Washington and California and a member of IEEE.

Emma Clawson received her BS in electrical engineering, summa cum laude, from Washington State University in 2021. In 2020 she was hired as an intern at Schweitzer Engineering Laboratories, Inc. (SEL), where she transitioned to working as a power engineer in 2021. She has also worked briefly for Avista Utilities as part of an engineering development exchange program between Avista Utilities and SEL.

Omar A. Oliveros received his BS in electrical engineering from Benemérita Universidad Autónoma de Puebla, Mexico. From 2005 to 2016, he worked as a protection engineer at Comisión Federal de Electricidad (CFE) where he performed electrical studies, protection schemes commissioning and testing, engineering design, and fault analysis in transmission and generation divisions. He joined Schweitzer Engineering Laboratories, S.A. de C.V. (SEL) in 2016 as a technical support protection application engineer for the Mexico central region and eventually the Central America and Caribbean regions as well. He presently works as a technology director of the Latin America region.

Jean León Eternod is a technology director for Schweitzer Engineering Laboratories, S.A. de C.V. (SEL) in Mexico. Prior to joining SEL in 1998, he worked for the Federal Electricity Commission (known in Mexico as CFE) power systems studies office in protection and control corporate management. While he was at CFE from 1991 to 1998, he worked with wide-area network protection schemes, single-pole tripping and reclosing studies, and database validation for short circuit, load flow, and dynamic simulation, including generator and control model validation for most CFE generators. He received his BSEE from the National Autonomous University of Mexico (known in Mexico as UNAM), where he also completed postgraduate course work in power systems. He received training in power system simulation from Power Technologies, Inc. He has authored numerous technical papers on the topics of power system protection, simulation, and wide-area protection and control applications.